JEM Journal of Experimental Medicine

ARTICLE

FOXO1 orchestrates the intestinal homeostasis via neuronal signaling in group 3 innate lymphoid cells

Fei Shao[1,2*], Zhen Liu[1,2*], Qinglin Wei[3,4*], Dou Yu[1,2], Min Zhao[1], Xusheng Zhang[1,2], Xintong Gao[1,2], Zusen Fan[5], and Shuo Wang[1,2]

The neuro-immune regulation is associated with homeostasis of the intestine. Intestinal group 3 innate lymphoid cells (ILC3s) are tissue-resident lymphocytes whose functions are affected by the intestine niche. However, how a gut neuronal signal coordinates the immune response of ILC3s is largely unknown. Here, we found that cyclic adenosine monophosphate (cAMP) signaling exacerbated the inflammatory response and attenuated the expression level of the transcription factor forkhead box O1 (FOXO1) in ILC3s. Deficiency of FOXO1 drove the hyperactivation of ILC3s and resulted in gut inflammation independently of T cells. Mechanistically, FOXO1 promoted the transcription of neuropeptide receptor VIPR2 and inhibited the transcription of adrenoceptor ADRA2A in ILC3s. FOXO1-related regulation of VIPR2 and ADRA2A signaling balanced the activation of ILC3s under steady condition or during colitis. Moreover, chronic stress elevated cAMP level and downregulated FOXO1 level, exacerbating intestinal inflammation. Our findings reveal that FOXO1 balances the activation of ILC3s via VIP and adrenergic signaling and regulates intestinal homeostasis.

Introduction

Innate lymphoid cells (ILCs) are abundant in mucosal surfaces to maintain mucosal homeostasis (Spits et al., 2013; Wang et al., 2017). ILC3s are characterized by retinoic acid–related orphan receptor γ t (RORγt) expression and interleukin (IL)-22 and IL-17 production, contributing to host defense against pathogens and barrier integrity in the intestine (Vivier et al., 2018). However, ILC3s play a double-edged-sword role in regulating intestinal inflammation. Excessive production of IL-17 and IL-22 leads to the over-reaction of neutrophils, exacerbating barrier damage and resulting in colitis (Zhou and Sonnenberg, 2020). Hyperactivation of ILC3s has been reported in patients with inflammatory bowel disease (IBD; Geremia et al., 2011). Increased expression of *IL17A* and *IL17F* was observed in the intestinal lamina propria ILC3s from patients with IBD compared with healthy donors. Human intestinal ILC3s produced increased levels of IL-22 in both patients with ulcerative colitis (UC) and those with Crohn's disease (CD) compared with the non-IBD individuals, indicating the dysfunction of ILC3s in IBD patients (Longman et al., 2014). On the other hand, ILC3s may also maintain intestine homeostasis. ILC3-derived heparin-binding epidermal growth factor–like growth factor is essential to protect the gut against TNF-mediated inflammation (Zhou et al., 2022). However, the balance of ILC3 function in intestine homeostasis is not well studied.

The intestine is innervated by millions of neurons, which modulate immune responses via secreting neurotransmitters and neuropeptides (Veiga-Fernandes and Mucida, 2016). The neuro-immune interactions play central roles in intestinal health and disease, including barrier integrity, host defense, and inflammatory conditions (Jacobson et al., 2021). The autonomic nervous system consists of the sympathetic nervous system, parasympathetic nervous system, and enteric nervous system, all of which are associated with gut immunity (Jakob et al., 2021; Udit et al., 2022). As the primary neurotransmitter of the sympathetic nervous system, noradrenaline plays an essential role in neuro-immune crosstalk (Lorton and Bellinger, 2015). Adrenergic receptors or adrenoceptors (Marino and Cosentino, 2013) mediate the physiological responses to noradrenaline and adrenalin, which also participate in inflammation and infection (Ahrends et al., 2021; Moriyama et al., 2018). For example, β2-AR (ADRB2) protects muscularis macrophages from neuronal loss during challenges with pathogens (Ahrends et al., 2021). ADRB2

[1]CAS Key Laboratory of Pathogen Microbiology and Immunology, Institute of Microbiology, Chinese Academy of Sciences, Beijing, China; [2]University of Chinese Academy of Sciences, Beijing, China; [3]Department of Gastroenterology, Seventh Medical Center of PLA General Hospital, Beijing, China; [4]Department of Cadre Diagnosis and Treatment, Seventh Medical Center of PLA General Hospital, Beijing, China; [5]CAS Key Laboratory of Infection and Immunity, CAS Center for Excellence in Biomacromolecules, Institute of Biophysics, Chinese Academy of Sciences, Beijing, China.

*F. Shao, Z. Liu, and Q. Wei contributed equally to this work. Correspondence to Shuo Wang: wangshuo@im.ac.cn.

prevents T helper 1 (Th1) cell development and promotes the differentiation of Th2, Th17, and regulatory T cells (Godinho-Silva et al., 2019). Recent studies showed that ILC2s expressed ADRB2, which was adjacent to adrenergic neurons. ADRB2 signaling inhibits the type 2 responses of ILC2s (Moriyama et al., 2018). In addition, enteric neurons are located within the myenteric plexus or the submucosal plexus close to immune cells such as goblet cells, macrophages, and ILCs (Jarret et al., 2020; Muller et al., 2014; Talbot et al., 2020; Wallrapp et al., 2017). The neuropeptide neuromedin U released from cholinergic neurons promotes the proliferation and activation of NMUR1$^+$ ILC2s (Wallrapp et al., 2017). Vasoactive intestinal peptide (VIP) produced by enteric neurons suppresses the production of inflammatory cytokines by ILC3s (Talbot et al., 2020). Diet is a way to regulate intestinal nerve system. Diets with glucosinolates promote IL-22 production by ILC3s and γδ T cells, and regulate the homeostasis of intestinal epithelial stem cells (Gronke et al., 2019). IL-22 is also critical to protect intestinal barrier against pathogenic bacteria infection (Lee et al., 2011). Stress is another way that contributes to neuronal regulation in the intestine. Depression and anxiety contribute to the onset or exacerbation of IBD (Bisgaard et al., 2022). Chronic stress is a potent risk factor for depressive disorder, and chronic restraint stress mouse models could produce depressive-like behavior and contribute to intestinal barrier dysfunction and inflammatory cell infiltration (Lee et al., 2021). Chronic stress contributes to gut microbiota disturbance, triggers immune responses, and exacerbates colitis (Gao et al., 2018). However, the regulation of neuropeptide receptors and neuronal signaling in ILC3s during colitis is rarely known.

The transcription factor FOXO1, a member of the forkhead box O (FOXO) family, is central to many physiological processes and modulated by the factors from tissue microenvironment (Hedrick et al., 2012). FOXO1 participates in regulating immune responses. Reports showed that FOXO1 maintains the quiescence state of naïve T cells and the function of regulatory T cells, and inhibits the proliferation of Th17 (Ichiyama et al., 2016), T follicular helper cells (Stone et al., 2015), and CD8$^+$ T cells (Delpoux et al., 2021). FOXO1 regulates the differentiation of B cells (Dominguez-Sola et al., 2015), activates M2 macrophages (Chung et al., 2019), and induces autophagy of natural killer (NK) cells during their maturation (Wang et al., 2016). Whether FOXO1 regulates the function of ILCs or ILC3s remains elusive. Cyclic adenosine monophosphate (cAMP) is an important second messenger participating in numerous physiological processes (Anton et al., 2022). cAMP also regulates the transcriptional activation of FOXO1 (Shen et al., 2014; Silveira et al., 2020). A previous report showed that cAMP inhibits ILC2 activation and proliferation (Wallrapp et al., 2019). However, other studies revealed that cAMP signaling can also promote the differentiation and activation of Th subsets and play a proinflammatory role (Hernandez et al., 2015; Li et al., 2012). The roles of cAMP and FOXO1 on ILC3s remain poorly understood.

In this study, we reveal neuronal signaling of ILC3s via the transcriptional activity of FOXO1. FOXO1 suppresses hyperactivation of ILC3s by balancing VIP and adrenergic signaling to maintain intestinal homeostasis.

Results

cAMP activates ILC3s and suppresses expression of FOXO1

cAMP as a second messenger is involved in many cellular processes and immune responses (Anton et al., 2022; Hernandez et al., 2015; Li et al., 2012; Shen et al., 2014; Silveira et al., 2020; Wallrapp et al., 2019). To explore the effect of cAMP on ILC3 functions, we isolated ILC3s from mouse small intestines and stimulated them with dibutyryl cAMP (d-cAMP), which mimics cAMP stimulation (Schwede et al., 2000). Although d-cAMP did not apparently promote the proliferation of ILC3s (Fig. 1 A), it significantly primed ILC3 activation in a dose-dependent manner. ILC3s produced elevated levels of IL-17A and IL-22 upon d-cAMP treatment (Fig. 1 B). In addition, d-cAMP increased the proportion and cell numbers of IL-17A–, IL-17F–, and IL-22–positive ILC3s (Fig. 1 C). Reports showed that cAMP modulated the transcriptional activities of many transcription factors, one of which is the FOXO family (Daitoku et al., 2004). cAMP promoted the phosphorylation of FOXO1 at Thr24, Ser256, and Ser319 residues, leading to nuclear export, inactivation, and degradation of FOXO1 (Liu et al., 2014; Silveira et al., 2020). Therefore, we next investigated the expression and activity of FOXO1 in ILC3s after d-cAMP treatment. Intriguingly, we found that d-cAMP decreased the levels of FOXO1 (Fig. 1 D) and promoted its phosphorylation (Fig. 1 E). Imaging flow cytometry revealed that FOXO1 of ILC3s translocated from the nucleus to cytosol upon d-cAMP treatment, suggesting the suppression of its transcriptional activity (Zaiss and Coffer, 2018; Fig. 1 F). These data indicated that d-cAMP elicited ILC3 activation and impaired the transcriptional activity of FOXO1.

FOXO1 prevents hyperactivation of ILC3s and attenuates colitis

We first employed *Foxo1*$^{flx/flx}$*;Rorc-Cre* mice to delete FOXO1 in RORγt-positive cells, including Th17 cells and ILC3s. We noticed that *Foxo1*$^{flx/flx}$*;Rorc-Cre* mice developed severe intestinal inflammation (Fig. S1, A–D). In addition, concentrations of inflammatory cytokines IL-17A and IL-22 in murine serum were significantly elevated in *Foxo1*$^{flx/flx}$*;Rorc-Cre* mice compared with littermate control mice (Fig. S1 E). Apart from the elevated activation of Th17 cells (Fig. S2, A and B), we found that ILC3s exhibited an inflammatory state and produced large amounts of inflammatory cytokines, including IL-17A, IL-17F, and IL-22 (Fig. S2, C and D). It was reported that *Citrobacter rodentium* (CR) infection could activate ILC3s and induce colitis before T cell activation (Jarade et al., 2021). We noticed that at early stage of CR infection, ILC3s were remarkably activated in *Foxo1*$^{flx/flx}$*;Rorc-Cre* mice (Fig. S2 D), indicating that FOXO1 might regulate ILC3s independently of T cells. In addition, reports showed that IL-17 and IL-22 recruited neutrophils via augmenting neutrophil-attractant chemokines (Zhou and Sonnenberg, 2020). Accordingly, we found that the proportion and numbers of neutrophils increased in the intestine of *Foxo1*$^{flx/flx}$*;Rorc-Cre* mice under physiological conditions or at an early stage of infection (Fig. S2 E).

To further exclude the effect of T cells, we used *Foxo1*$^{flx/flx}$*;Rorc-Cre;Rag1*$^{-/-}$ mice to evaluate the role of FOXO1 in ILC3s. Similar to that in T cell–intact mice, the small intestine and colon

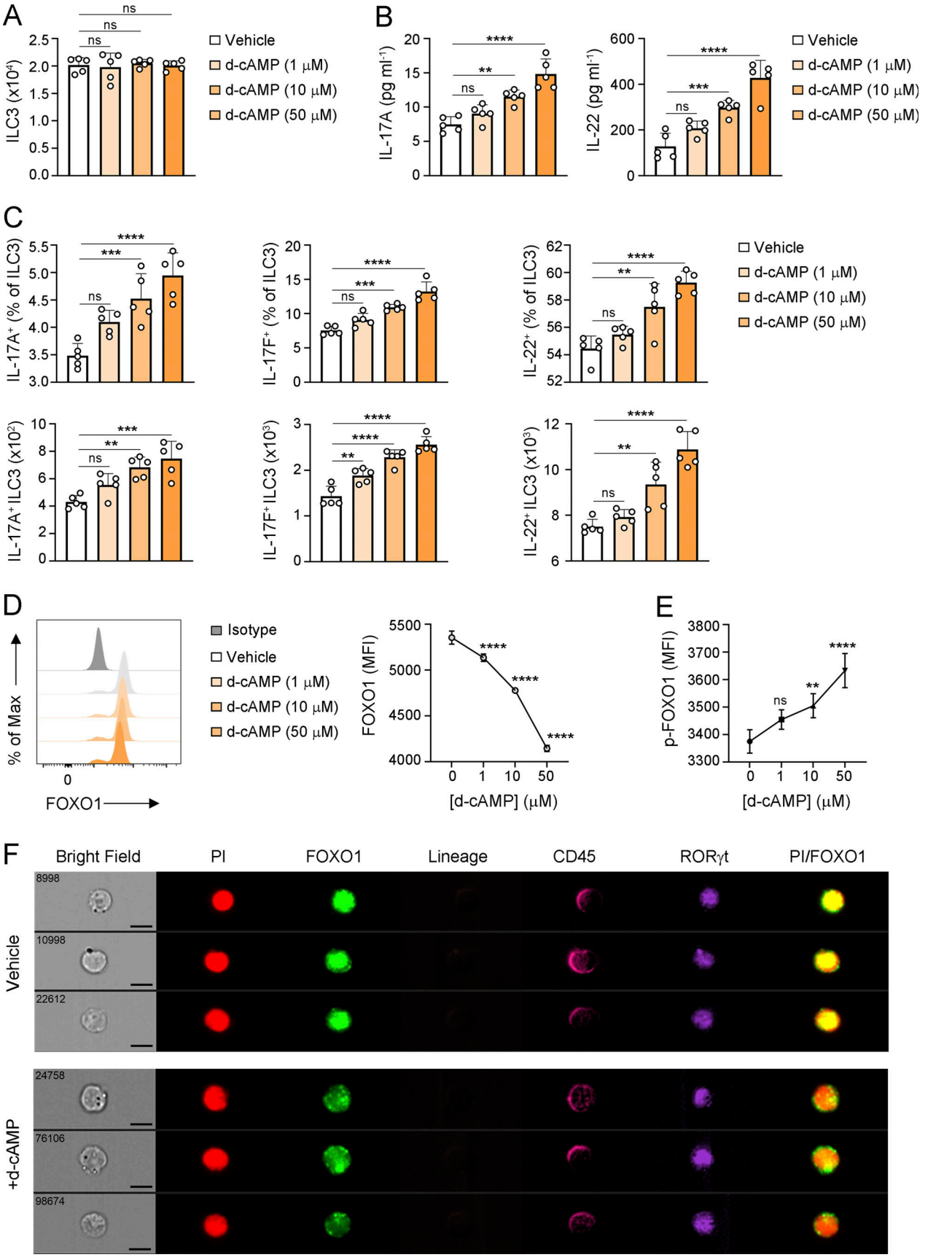

Figure 1. **d-cAMP promotes ILC3 activation and suppresses the expression and activity of FOXO1. (A)** Proliferation of ILC3s was not affected by d-cAMP treatment. Viable ILC3s (Lin⁻NK1.1⁻KLRG1⁻CD45^{low}CD127⁺CD90.2^{hi}, Lin = CD3, CD19, CD11b, CD11c, Gr-1, TER-119, TCRβ, TCRγδ) were isolated from the

lamina propria of the small intestine of WT mice and treated with vehicle or the indicated concentrations of d-cAMP in RPMI1640 complete medium supplemented with 25 ng ml^{-1} IL-7 and 25 ng ml^{-1} IL-23 for 16 h. The cell counts of ILC3s were analyzed by flow cytometry and shown as means ± SD. ns, not significant, by one-way ANOVA. *n* = 5 for each group. **(B)** d-cAMP promoted the activation of ILC3s. The isolated ILC3s were treated with the indicated concentrations of d-cAMP. The levels of IL-17A and IL-22 in supernatant of cell culture were analyzed by ELISA and shown as means ± SD. ns, not significant, **, P < 0.01, ***, P < 0.001, ****, P < 0.0001, by one-way ANOVA. *n* = 5 for each group. **(C)** d-cAMP elevated the levels of inflammatory cytokines of ILC3s. The isolated ILC3s were treated with the indicated concentrations of d-cAMP. The proportion and numbers of IL-17A–, IL-17F–, and IL-22–positive ILC3s were analyzed by flow cytometry and shown as means ± SD. ns, not significant, **, P < 0.01, ***, P < 0.001, ****, P < 0.0001, by one-way ANOVA. *n* = 5 for each group. (ILC3 = $Lin^-NK1.1^-KLRG1^-CD45^+CD127^+ROR\gamma t^+$, Lin = CD3, CD19, CD11b, CD11c, Gr-1, TER-119, TCRβ, TCRγδ). **(D and E)** d-cAMP decreased the level of FOXO1 and promoted its phosphorylation. The isolated ILC3s were treated with the indicated concentrations of d-cAMP. Medians of fluorescence intensity (MFI) of FOXO1 (D) and phosphorylated FOXO1 (p-FOXO1) in ILC3s (E) were determined by flow cytometry and shown as means ± SD. The representative flow cytometry plots are shown on the left. ns, not significant, **, P < 0.01, ****, P < 0.0001, by one-way ANOVA. *n* = 5 for each group. **(F)** ILCs in small intestine from WT mice were isolated by Magnetic Cell Sorting system (BioLegend) and treated with vehicle or d-cAMP (50 μM) for 16 h. ILCs were stained with propidium iodide (PI) for cell nucleus and antibodies against FOXO1, Lin (CD3, CD19, CD11b, CD11c, Gr-1, TER-119, TCRβ, TCRγδ, NK1.1, and KLRG1), CD45, and RORγt. The FOXO1 nuclear translocation was examined by imaging flow cytometry. Scale bar, 5 μm. *n* = 5 for each group. Data represent at least three independent experiments.

showed more severe intestinal ulceration, a significant increase in mucosal thickness and leukocyte infiltration, and shortened colon length in *Foxo1*$^{flx/flx}$*;Rorc-Cre;Rag1*$^{-/-}$ mice (Fig. 2, A–C). These results manifested the gut inflammation in *Foxo1*$^{flx/flx}$*;Rorc-Cre;Rag1*$^{-/-}$ mice (Lelievre et al., 2007). In the absence of T and B cells, CR infection induced ILC3-dependent colitis, and FOXO1 abrogation in ILC3s also aggravated CR-induced colitis (Fig. 2, A–C). In addition, we found that the serum levels of IL-17A and IL-22 were elevated in *Foxo1*$^{flx/flx}$*;Rorc-Cre;Rag1*$^{-/-}$ mice under physiological condition or during CR-induced colitis (Fig. S2 F). However, the frequencies and total numbers of ILC3s in small intestine and mesenteric lymph nodes did not significantly change (Fig. 2 D). Consistent with the results from *Foxo1*$^{flx/flx}$*;Rorc-Cre* mice, the numbers and frequencies of IL-17A$^+$, IL-17F$^+$, and IL-22$^+$ ILC3s increased in the small intestine and mesenteric lymph nodes of *Foxo1*$^{flx/flx}$*;Rorc-Cre;Rag1*$^{-/-}$ mice (Fig. 2 E). Similar results were observed in mice infected with CR. On day 8 after infection, ILC3s in *Foxo1*$^{flx/flx}$*;Rorc-Cre;Rag1*$^{-/-}$ mice produced extremely high levels of inflammatory cytokines, including IL-17A, IL-17F, and IL-22 (Fig. 2 E). Accordingly, neutrophils were remarkably augmented in the intestine of *Foxo1*$^{flx/flx}$*;Rorc-Cre;Rag1*$^{-/-}$ mice (Fig. 2 F). Collectively, these findings suggested that FOXO1 contributed to the suppression of the inflammatory response of ILC3s.

FOXO1 regulates expression levels of α 2 adrenergic receptor (ADRA2A) and VIPR2 on ILC3s

To gain insights into the regulated network by FOXO1 that differs between ILC3s and T cells, we isolated ILC3s and CD3$^+$ T cells from intestinal lamina propria of *Foxo1*$^{flx/flx}$*;Rorc-Cre* mice and littermate control mice and examined the transcriptomic change using single-cell RNA sequencing (scRNA-seq). We selected *Rorc*-positive cells for clustering. The unsupervised clustering partitioned the cells into four clusters, including Th17, CCR6$^+$ ILC3, NCR1$^+$ ILC3, and NKT17 (Fig. 3 A and Fig. S3 A). We analyzed the differential gene expression between the control and *Foxo1*$^{flx/flx}$*;Rorc-Cre* mice under steady state or during CR-induced colitis. Volcano plots showed that in *Foxo1*-deficient ILC3s, the expression of inflammatory cytokine genes, including *Il17a*, *Il17f*, and *Il22*, significantly increased, while some other genes, including *Il10*, *Ret*, and *Vipr2*, were downregulated (Fig. 3 B). Next, we employed gene set enrichment analysis on the differential expressed genes and found that colitis-related genes were enriched in *Foxo1*-defecient ILC3s (Fig. 3 C; Kibbe et al., 2015), which was consistent with our previous data.

Since the hyperactivation of ILC3s was also observed in *Rag1*$^{-/-}$ mice, we intended to find out the unique transcriptional network orchestrated by FOXO1 in ILC3s independent of T cells. We next picked out the genes specifically expressed in ILC3s and changed after FOXO1 depletion (Fig. 3 D). The differentially expressed genes (DEGs) in *Foxo1*-deficient ILC3s belonged to the pathways in IBD, cAMP signaling, and neuro-associated signaling (Fig. 3 E and Fig. S3 B). Among these, we selected the genes that changed the most in *Foxo1*-deficient ILC3s, including the upregulated adrenergic receptor gene *Adra2a* and downregulated VIP receptor gene *Vipr2* (Fig. 3 F). Notably, the expression level of *Adra2a* increased in CR-infected mice and was extremely high in *Foxo1*-deficient ILC3s after infection (Fig. 3 F). On the contrary, the expression of *Vipr2* was attenuated after CR infection and was even lower with FOXO1 abrogation (Fig. 3 F). We further confirmed the expression of *Adra2a* and *Vipr2* in ILC3s, mainly in CCR6$^+$ ILC3s, but not in Th17 cells (Fig. 3 G). Notably, the expression levels of other adrenergic receptors or VIP receptors were very low or undetectable in ILC3s (Fig. 3 G and Fig. S3 C). The expression of *Il17a*, *Il17f*, and *Il22* was correlated with that of *Adra2a*, but opposite to that of *Vipr2* (Fig. 3 H). Additionally, we analyzed the scRNA-seq data of IBD patients (Smillie et al., 2019) and observed that the expression levels of *FOXO1* and *VIPR2* were higher in the intestine of healthy people, and the levels of *ADRA2A* and *IL17A* were augmented in the intestine of IBD patients (Fig. S3 D). Collectively, FOXO1 differentially regulated adrenoceptors and neuropeptide receptors on ILC3s, which might contribute to the regulation of intestinal homeostasis.

FOXO1 directly targets the promoters of *Adra2a* and *Vipr2* genes

To determine the molecular network regulated by FOXO1 in ILC3s, we evaluated the transcription and expression of *Adra2a* and *Vipr2* in *Foxo1*-deficient ILC3s. Consistent with scRNA-seq data, the transcription and expression of *Adra2a* were elevated in *Foxo1*$^{-/-}$ ILC3s, and those of *Vipr2* were attenuated with FOXO1 abrogation (Fig. 4, A and B). CR infection decreased the level of FOXO1 accompanied by upregulation of *Adra2a* and downregulation of *Vipr2* (Fig. S3 E and Fig. 4, A and B), indicating a dynamic regulation of

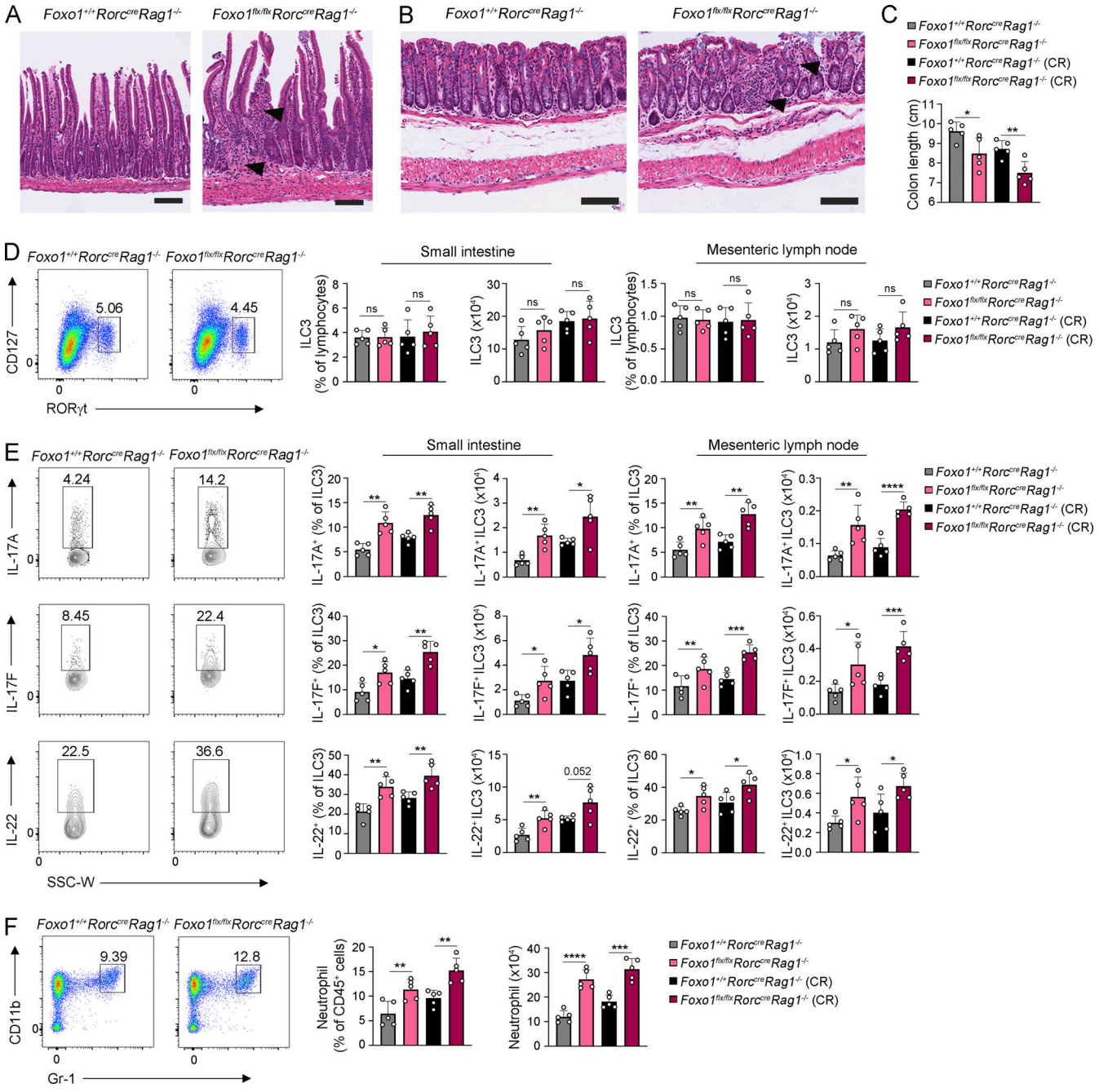

Figure 2. **FOXO1 deficiency causes hyperactivation of ILC3s and intestinal inflammation. (A and B)** FOXO1 deficiency in ILC3s contributed to colitis. Representative H&E-stained sections of the small intestine (A) and colon (B) from *Foxo1*$^{+/+}$*;Rorc-Cre;Rag1*$^{-/-}$ mice and *Foxo1*$^{flx/flx}$*;Rorc-Cre;Rag1*$^{-/-}$ mice. Arrowheads indicate inflammatory lesions. Scale bars, 100 µm. **(C)** Comparison of the colon length between the control and *Foxo1*$^{flx/flx}$*;Rorc-Cre;Rag1*$^{-/-}$ mice. *Foxo1*$^{+/+}$*;Rorc-Cre;Rag1*$^{-/-}$ mice and *Foxo1*$^{flx/flx}$*;Rorc-Cre;Rag1*$^{-/-}$ mice were orally gavaged with or without of 2 × 10^9 CFU of CR. After 8 d, the colon length of the indicated mice was measured and shown as means ± SD. *, P < 0.05, **, P < 0.01, by two-tailed unpaired Student's *t* test. *n* = 5 for each group. **(D)** FOXO1 deficiency did not promote the proliferation of ILC3s. The proportion and numbers of ILC3s in the small intestine and mesenteric lymph nodes from indicated mice treated as above were analyzed by flow cytometry and shown as means ± SD. The representative flow cytometry plots of lamina propria ILC3s from uninfected mice are shown on the left panel. ns, not significant, by two-tailed unpaired Student's *t* test. *n* = 5 for each group. **(E)** FOXO1 deficiency elevated the activation of ILC3s. The proportion and numbers of IL-17A–, IL-17F–, and IL-22–positive ILC3s from the small intestine and mesenteric lymph nodes of *Foxo1*$^{+/+}$*;Rorc-Cre;Rag1*$^{-/-}$ mice and *Foxo1*$^{flx/flx}$*;Rorc-Cre;Rag1*$^{-/-}$ mice were analyzed by flow cytometry and shown as means ± SD (right panel). The representative flow cytometry plots of lamina propria ILC3s from uninfected mice are shown on the left panel. *, P < 0.05, **, P < 0.01, ***, P < 0.001, ****, P < 0.0001, by two-tailed unpaired Student's *t* test. *n* = 5 for each group. **(F)** FOXO1 deficiency in ILC3s promoted neutrophil recruitment in the intestine. The proportion and numbers of neutrophils in small intestine from *Foxo1*$^{+/+}$*;Rorc-Cre;Rag1*$^{-/-}$ mice and *Foxo1*$^{flx/flx}$*;Rorc-Cre;Rag1*$^{-/-}$ mice were analyzed by flow cytometry and shown as means ± SD. The representative flow cytometry plots of lamina propria neutrophils from uninfected mice are shown on the left panel. **, P < 0.01, ***, P < 0.001, ****, P < 0.0001, by two-tailed unpaired Student's *t* test. *n* = 5 for each group. ILC3 = Lin$^-$NK1.1$^-$KLRG1$^-$CD45$^+$CD127$^+$RORγt$^+$ (Lin = CD3, CD19, CD11b, CD11c, Gr-1, TER-119, TCRβ, TCRγδ). Neutrophil = CD3$^-$CD19$^-$CD45$^+$CD11b$^+$Gr-1$^+$. Data represent at least three independent experiments.

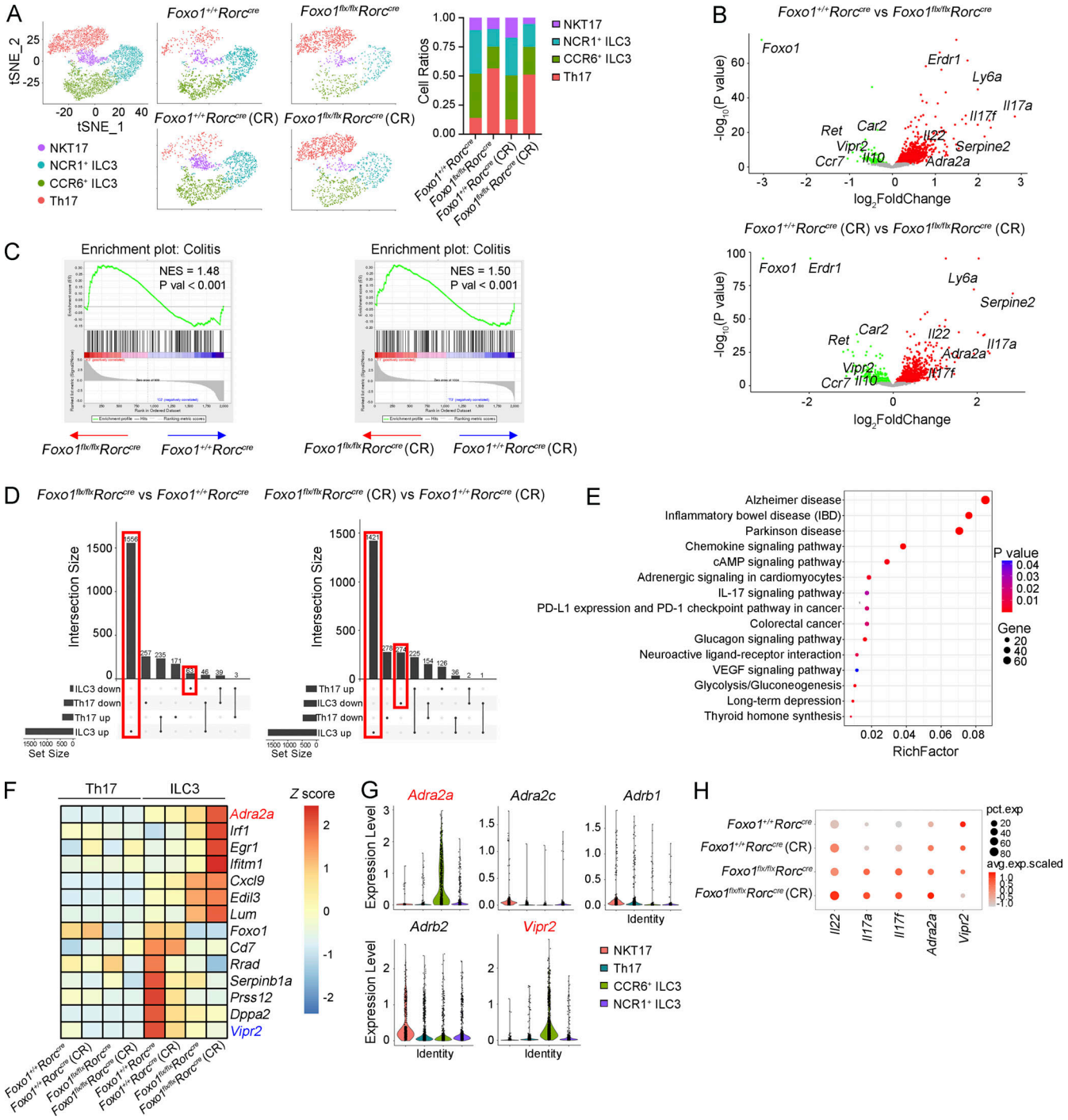

Figure 3. **FOXO1 regulates expression of ADRA2A and VIPR2 in ILC3s. (A)** scRNA-seq revealed the subpopulation of ILC3s and Th17 cells. CD3$^+$ cells (Lin$^-$CD45.2$^+$CD3$^+$, Lin = CD19, CD11b, CD11c, TER-119, Gr-1) and ILC3s (Lin$^-$CD3$^-$CD45^{low}CD127$^+$CD90^{hi}) from small intestine lamina propria of *Foxo1*$^{+/+}$;*Rorc-Cre* mice and *Foxo1*$^{flx/flx}$;*Rorc-Cre* mice with or without CR infection were isolated and examined using scRNA-seq. The scRNA-seq yielded 32,028 quality cells in this study. The quality control metrics in this study are shown in Table S1. *Rorc*-positive cells were selected out and clustered partitioned into four clusters, including Th17, CCR6$^+$ ILC3, NCR1$^+$ ILC3, and NKT17 according to their signature genes (Fig. S3 A; *n* = 1,580 for *Foxo1*$^{+/+}$;*Rorc-Cre* group; *n* = 1,143 for *Foxo1*$^{flox/flox}$;*Rorc-Cre* group; *n* = 1,570 for *Foxo1*$^{+/+}$;*Rorc-Cre* [CR] group; *n* = 1,527 for *Foxo1*$^{flx/flx}$;*Rorc-Cre* [CR] group). The cell ratios of the indicated clusters are shown in the right panel. **(B)** Volcano plot of DEGs in ILC3s between control and *Foxo1*$^{flx/flx}$;*Rorc-Cre* mice. EdgeR (version 3.26.8) was used for DEG analysis (Li et al., 2022; Squair et al., 2021). Red dots represented the genes highly expressed in ILC3s of *Foxo1*$^{flx/flx}$;*Rorc-Cre* mice, and green dots represent the genes highly expressed in ILC3s of *Foxo1*$^{+/+}$;*Rorc-Cre* mice. **(C)** GSEA of DEGs upregulated in *Foxo1*-deficient ILC3s compared with those of control ILC3s. Colitis-related genes (Table S2) were enriched in *Foxo1*-deficient ILC3s. Empirical P values and normalized enrichment score (NES) are shown. **(D)** Upset plot for the ILC3 and Th17 cell DEGs between *Foxo1*$^{+/+}$;*Rorc-Cre* mice and *Foxo1*$^{flx/flx}$;*Rorc-Cre* mice with or without CR infection. The columns highlighted with red rectangles were gene numbers specifically up- or downregulated in *Foxo1*$^{-/-}$ ILC3s. **(E)** Enrichment analysis of Kyoto Encyclopedia of Genes and Genomes pathways for DEGs only in ILC3s, not in Th17 cells of *Foxo1*$^{flx/flx}$;*Rorc-Cre* mice versus *Foxo1*$^{+/+}$;*Rorc-Cre* mice. RichFactor = (the number of DEGs)/(total number of genes). **(F)** Expression heatmap of

the indicated genes in ILC3s and Th17 cells of *Foxo1*$^{+/+}$;*Rorc-Cre* mice and *Foxo1*$^{flx/flx}$;*Rorc-Cre* mice with or without CR infection. **(G)** Expression levels of adrenergic receptor genes and *Vipr2* gene in the indicated cell clusters were visualized in the violin plots. **(H)** Dot plot showing the mean expression levels of the indicated genes in ILC3s from *Foxo1*$^{+/+}$;*Rorc-Cre* mice and *Foxo1*$^{flx/flx}$;*Rorc-Cre* mice with or without CR infection. The dot size represents the proportion of cells that expressed the indicated genes. The color represented the average expression level of indicated genes across ILC3s. Data represent at least two independent experiments.

FOXO1 activity during CR-induced colitis. In addition, we verified these results in *Foxo1*$^{flx/flx}$;*Rorc-Cre;Rag1*$^{-/-}$ mice (Fig. 4 C). Next, we performed CUT&Tag assay followed by high-throughput sequencing to identify the FOXO1 DNA-binding sites on the genome of ILC3s. We found that FOXO1 directly bound to the promoters of *Adra2a* and *Vipr2* with multiple binding sites (Fig. 4, D and E). The binding regions of FOXO1 were confirmed by chromatin immunoprecipitation–quantitative PCR (ChIP-qPCR; Fig. 4 F). During CR-induced colitis, the binding of FOXO1 on the promoters of *Adra2a* and *Vipr2* was impaired suggesting the suppression of its regulatory function by CR infection (Fig. 4 G). Luciferase reporter assay revealed the transcriptional suppression of *Adra2a* and the transcriptional activation of *Vipr2* by FOXO1 in ILC3s (Fig. 4 H). We also mapped the target regions of FOXO1 on these promoters by using various tractions. We found that −1389 to −940 bp region of the *Adra2a* promoter was occupied by FOXO1, which suppressed its transcription. Additionally, FOXO1 bound to −1539 to −1290 bp region of the *Vipr2* promoter and promoted its expression (Fig. 4 H). These data suggested that FOXO1 directly targeted the promoters of *Adra2a* and *Vipr2* and regulated their transcription.

ADRA2A and VIPR2 signaling pathways balance the effector function of ILC3s

It was reported that food consumption promoted VIP production in the intestine and attenuated the activation of ILC3s (Talbot et al., 2020). Short-term VIP treatment alleviated CR-induced colitis in mice (Conlin et al., 2009). The function of ADRA2A signaling in ILC3s has not been analyzed. First, we used immunofluorescence to analyze the location of neurons and ILC3s and found there was anatomical correlation between the neurons and ILC3s in the small intestine under steady state or during CR-induced colitis (Fig. S3 F). We next explored how ADRA2A and VIPR2 signaling pathways affected the function of ILC3s. After treatment with ADRA2A agonist clonidine, levels of IL-17A and IL-22 of ILC3s apparently increased in vitro (Fig. 5 A). Similar results were obtained after the inhibition of VIP signaling (Fig. 5 B). To further analyze the effect of ADRA2A and VIPR2 signaling in ILC3s in vivo, we treated the mice with ADRA2A agonist clonidine or VIPR2 antagonist PG99-465 intraperitoneally (i.p.). We found that ADRA2A agonist or VIPR2 antagonist apparently increased the frequency and number of IL-17– and IL-22–producing ILC3s (Fig. 5, C and D). Notably, ADRA2A antagonist or VIPR2 agonist apparently attenuated the inflammation response of ILC3s (Fig. S3, G and H). Next, we conditionally knocked out *Adra2a* gene in ILC3s. Since RORγt-positive T cells did not express *Adra2a* (Fig. 3 G), *Adra2a*$^{flx/flx}$;*Rorc*^{cre} mice could be used to analyze the function of ADRA2A in ILC3s. Importantly, depletion of *Adra2a* in ILC3s reduced the production of inflammatory cytokines in ILC3s, including IL-17A, IL-17F, and IL-22 (Fig. 5 E). Accordingly, the inflammation of the intestine was attenuated in *Adra2a*$^{flx/flx}$;*Rorc*^{cre} mice after CR infection (Fig. 5 F). Notably, treatment with ADRA2A antagonist and VIPR2 agonist successfully attenuated the hyperactivation of ILC3s in *Foxo1*$^{flx/flx}$;*Rorc-Cre* mice (Fig. 5 G). These data collectively suggested that ADRA2A and VIPR2 neuronal signalings differentially regulated the function of ILC3s.

Chronic stress induces hyperactivation of ILC3s and intestinal inflammation via cAMP–FOXO1 axis

ADRA2A signaling is known to be associated with stress responses (Laarakker et al., 2010). Accumulating evidence showed that stress is a potential predisposing factor for gut disorders, such as IBD or irritable bowel syndrome (Gao et al., 2018; Sun et al., 2019). The crosstalk between stress-related neuronal signaling and immune responses during colitis is not well known. It was reported that stress can activate the cAMP–protein kinase A signaling pathway (Thaker et al., 2006). We then investigated whether chronic stress exacerbated gut inflammation via cAMP–FOXO1 axis using a chronic restraint stress model (Gao et al., 2018; Li et al., 2020). The mice under stress exhibited decreased body weight and increased immobility times compared with those in the control group, indicating depression-like behavior (Fig. 6, A–C). The stressed mice showed more severe intestinal damage and increased villus height and crypt depth but decreased colon length (Fig. 6, D and E). Consistent with the previous reports (Thaker et al., 2006), chronic stress elevated cAMP levels in serum (Fig. 6 F). Of note, we found that chronic stress decreased the level of FOXO1 in ILC3s accompanied by its phosphorylation (Fig. 6, G and H). In addition, expression levels of ADRA2A were elevated and expression of VIPR2 was repressed in stressed mice (Fig. 6 I). We next examined the effect of chronic stress on the function of ILC3s. ILC3s in the stressed mice produced larger amounts of inflammatory cytokines under steady state or during CR-induced colitis (Fig. 6 J). Moreover, the ADRA2A antagonist Yohimbine treatment could remedy ILC3-dependent inflammatory response induced by stress (Fig. S3 I). Then, we set up a stress mouse model by using *Foxo1*$^{flx/flx}$;*Rorc-Cre;Rag1*$^{-/-}$ mice and found that the proportion of IL-17A–, IL-17F–, and IL-22–positive ILC3s were not affected by stress treatment (Fig. S3 J), suggesting that stress-related inflammatory response of ILC3s is FOXO1 dependent. We further investigated whether the neuro-associated pathways of ILC3s were regulated by cAMP–FOXO1 axis in IBD patients. We found that the IBD patients had higher self-rating depression scale scores (Fig. 6 K) and elevated serum cAMP levels (Fig. 6 L). Consistently, expression levels of *FOXO1* and *VIPR2* were downregulated and expression levels of *ADRA2A* were increased in IBD patients (Fig. 6 M). The proportion of IL-17A^{+}, IL-22^{+} ILC3s, and neutrophils were elevated in the intestine from IBD patients compared with healthy donors (Fig. 6, N and O).

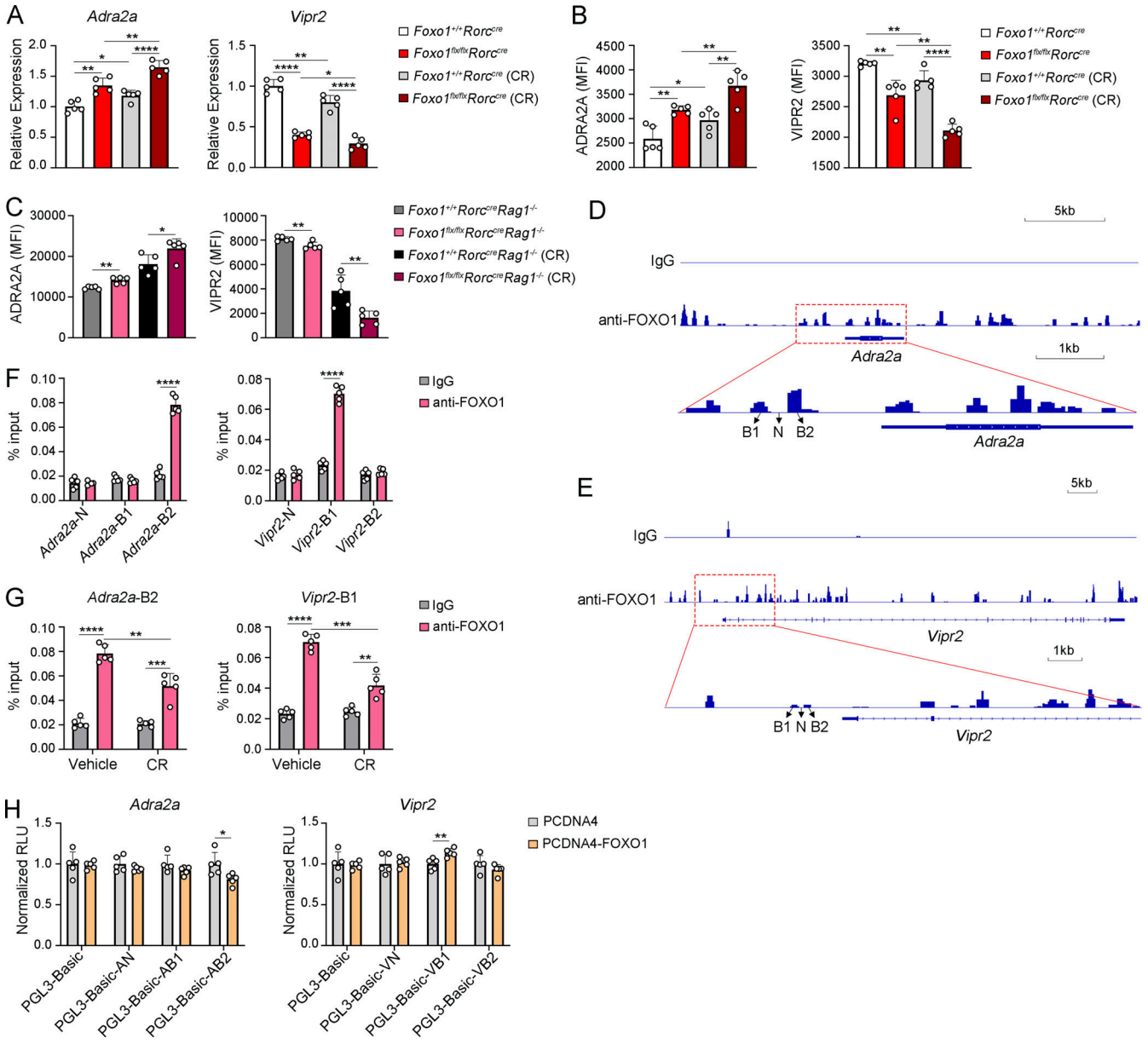

Figure 4. **FOXO1 modulates transcription of *Adra2a* and *Vipr2* by targeting their promoters. (A)** Expression levels of *Adra2a* and *Vipr2* genes in *Foxo1*-deficient ILC3s. Real-time qPCR analysis of *Adra2a* and *Vipr2* in ILC3s (Lin$^-$NK1.1$^-$KLRG1$^-$CD45^{low}CD127$^+$CD90.2^{hi}) isolated from small intestine of *Foxo1*$^{+/+}$*;Rorc-Cre* mice and *Foxo1*$^{flx/flx}$*;Rorc-Cre* mice with or without CR infection. Values were normalized to housekeeping gene *Gapdh*. The relative expression of indicated genes was calculated and shown as means ± SD. *, P < 0.05, **, P < 0.01, ****, P < 0.0001, by two-tailed unpaired Student's *t* test. *n* = 5 for each group. **(B)** Protein levels of ADRA2A and VIPR2 on ILC3 from *Foxo1*$^{+/+}$*;Rorc-Cre* mice and *Foxo1*$^{flx/flx}$*;Rorc-Cre* mice with or without CR infection were analyzed by flow cytometry and MFI are shown as means ± SD. *, P < 0.05, **, P < 0.01, ****, P < 0.0001, by two-tailed unpaired Student's *t* test. *n* = 5 for each group. **(C)** Expression of ADRA2A and VIPR2 on ILC3s from *Foxo1*$^{+/+}$*;Rorc-Cre;Rag1*$^{-/-}$ mice and *Foxo1*$^{flx/flx}$*;Rorc-Cre;Rag1*$^{-/-}$ mice with or without CR infection were analyzed by flow cytometry, and MFI are shown as means ± SD. *, P < 0.05, **, P < 0.01, by two-tailed unpaired Student's *t* test. *n* = 5 for each group. **(D and E)** FOXO1 occupancy at *Adra2a* and *Vipr2* gene promoter loci in ILC3s. ILC3s were isolated from the intestine of WT mice and subjected to CUT&Tag experiment, which was described in the Materials and methods section. Briefly, ILC3s from WT mice were treated with anti-FOXO1 or anti-IgG antibodies and Tn5 transposon followed by DNA sequencing. The promoters of *Adra2a* (D) and *Vipr2* (E) occupied by FOXO1 are shown. B1, binding region 1; N, negative control region; B2, binding region 2. **(F)** The FOXO1-binding regions of *Adra2a* and *Vipr2* promoters were verified in ILC3s of WT mice by ChIP-qPCR. The precipitated regions by anti-FOXO1 antibody were analyzed and shown as means ± SD. ****, P < 0.0001, by two-tailed unpaired Student's *t* test. *n* = 5 for each group. Anti-IgG served as a negative control. **(G)** Binding of FOXO1 on *Adra2a* and *Vipr2* gene promoter was impaired by CR infection. ILC3s were isolated from mice with or without CR infection. Binding of FOXO1 on B2 region of *Adra2a* promoter and B1 region of *Vipr2* promoter were analyzed by ChIP-qPCR. **, P < 0.01, ***, P < 0.001, ****, P < 0.0001, by two-tailed unpaired Student's *t* test. *n* = 5 for each group. **(H)** The transcription of *Adra2a* genes (left) or *Vipr2* genes (right) were regulated by FOXO1. The pcDNA4-mouse FOXO1 vector and luciferase reporter vectors (pGL3) containing the mouse *Adra2a* promoter or *Vipr2* promoter were transfected into HEK293T cells followed by dual-luciferase reporter assay. pGL3 vector served as a negative control. The relative luciferase units (RLUs) were calculated and shown as means ± SD, *, P < 0.05, **, P < 0.01, by two-tailed unpaired Student's *t* test. *n* = 5 for each group. RLUs of firefly luciferase activity were normalized to Renilla luciferase activity. Data represent at least three independent experiments.

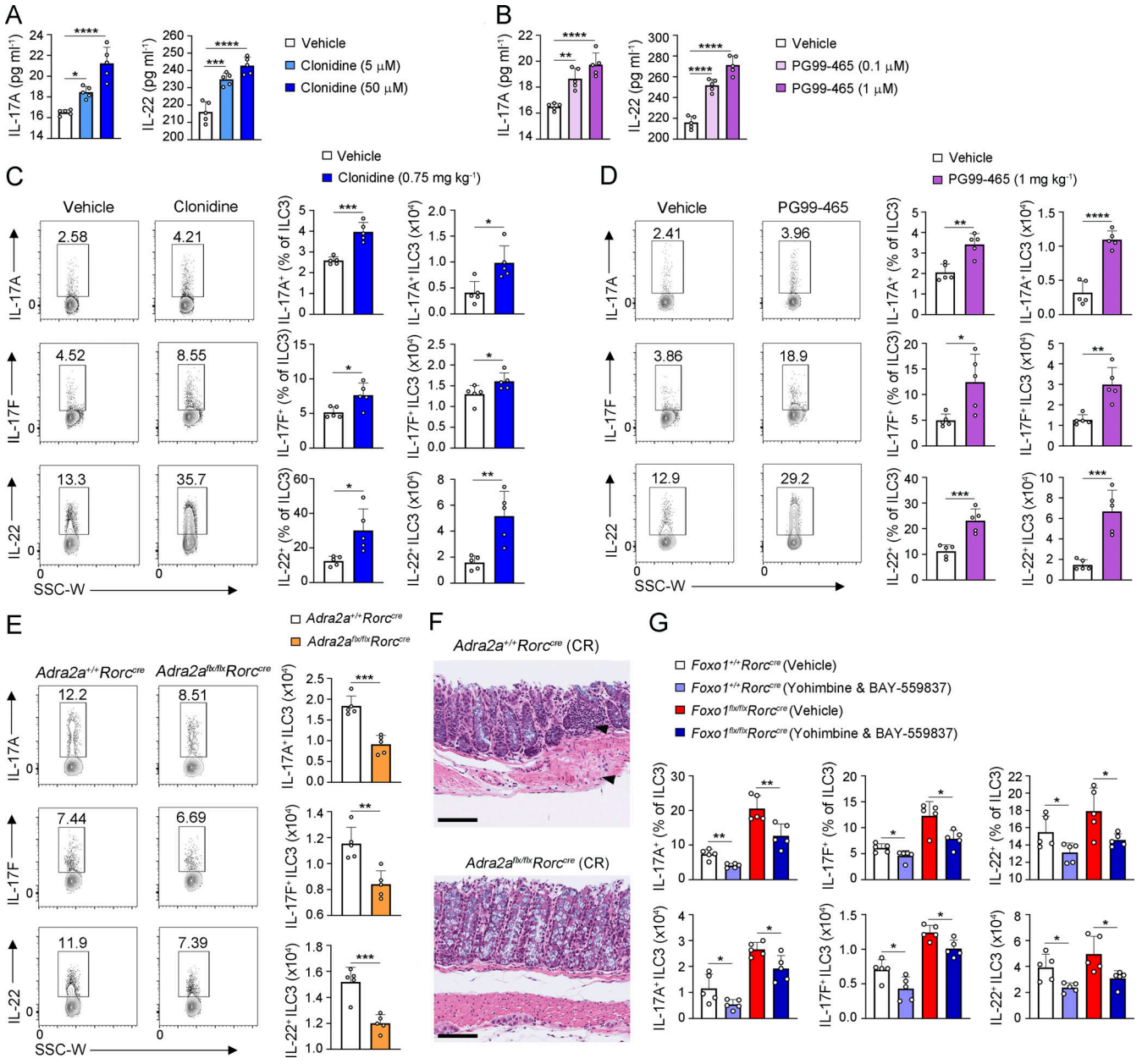

Figure 5. **ADRA2A and VIPR2 signaling pathways balance the activation of ILC3s. (A)** The activation of ILC3 was induced by ADRA2A agonist. 5 × 10^4 ILC3s from the small intestine of WT mice were cultured in the presence of IL-7 (25 ng ml^{-1}), IL-23 (25 ng ml^{-1}), and ADRA2A agonist clonidine (5 or 50 μM) for 16 h. The supernatant levels of IL-17A and IL-22 were determined by ELISA and shown as means ± SD. *, P < 0.05, ***, P < 0.001, ****, P < 0.0001, by one-way ANOVA. *n* = 5 for each group. **(B)** The activation of ILC3s was elevated by VIPR2 antagonist. 5 × 10^4 intestinal ILC3s from WT mice were cultured in the presence of IL-7 (25 ng ml^{-1}), IL-23 (25 ng ml^{-1}), and VIPR2 antagonist PG99-465 (0.1 or 1 μM) for 16 h. IL-17A and IL-22 levels of the culture supernatants were determined by ELISA and shown as means ± SD. **, P < 0.01, ****, P < 0.0001, by one-way ANOVA. *n* = 5 for each group. **(C)** WT mice were i.p. injected with vehicle or ADRA2A agonist clonidine (0.75 mg kg^{-1} mouse) and sacrificed after 24 h. The proportion and cell numbers of IL-17A–, IL-17F–, and IL-22–positive ILC3s from the small intestine were determined by flow cytometry and shown as means ± SD. The representative flow cytometry plots of intestinal ILC3s are shown on the left panel. *, P < 0.05, **, P < 0.01, ***, P < 0.001, by two-tailed unpaired Student's *t* test. *n* = 5 for each group. **(D)** Mice were treated with vehicle or VIPR2 antagonist PG99-465 (1 mg kg^{-1} mouse) via i.p. injection and sacrificed after 24 h. The proportion and numbers of IL-17A–, IL-17F–, and IL-22–positive ILC3s from the small intestine were determined by flow cytometry and shown as means ± SD. The representative flow cytometry plots of intestinal ILC3s are shown on the left panel. *, P < 0.05, **, P < 0.01, ***, P < 0.001, ****, P < 0.0001, by two-tailed unpaired Student's *t* test. *n* = 5 for each group. **(E)** Suppression of ILC3 activation in *Adra2a*$^{flx/flx}$*;Rorc-cre* mice. The numbers of IL-17A–, IL-17F–, and IL-22–positive ILC3s in the small intestine from *Adra2a*$^{+/+}$*;Rorc-cre* mice and *Adra2a*$^{flx/flx}$*;Rorc-cre* mice were analyzed by flow cytometry and shown as means ± SD. The representative flow cytometry plots of intestinal ILC3s are shown on the left panel. **, P < 0.01, ***, P < 0.001, by two-tailed unpaired Student's *t* test. *n* = 5 for each group. **(F)** ADRA2A deficiency in ILC3s attenuated intestinal inflammation. Representative H&E-stained sections of the colon from *Adra2a*$^{+/+}$*;Rorc-Cre* mice and *Adra2a*$^{flx/flx}$*;Rorc-Cre* mice with CR infection. Arrowheads indicated the inflammatory lesions. Scale bars, 100 μm. **(G)** Suppression of hyperactivation of *Foxo1*$^{-/-}$ ILC3s by targeting ADRA2A and VIPR2 pathways. To suppress the hyperactivation of ILC3s caused by FOXO1 deficiency, *Foxo1*$^{+/+}$*;Rorc-Cre* mice and *Foxo1*$^{flx/flx}$*;Rorc-Cre* mice were injected i.p. with vehicle or mixture of ADRA2A antagonist Yohimbine (1 mg kg^{-1} mouse) and VIPR2 agonist BAY-559837 (1 mg kg^{-1} mouse) and sacrificed after 24 h. The proportion and

numbers of IL-17A–, IL-17F–, and IL-22–positive ILC3s were analyzed by flow cytometry and shown as means ± SD. *, P < 0.05, **, P < 0.01, by two-tailed unpaired Student's *t* test. *n* = 5 for each group. Gate strategy for viable ILC3 sorting was Lin$^-$NK1.1$^-$KLRG1$^-$CD45^{low}CD127$^+$CD90.2^{hi}. Gate strategy for ILC3 analysis was Lin$^-$NK1.1$^-$KLRG1$^-$CD45$^+$CD127$^+$RORγt$^+$ (Lin = CD3, CD19, CD11b, CD11c, Gr-1, TER-119, TCRβ, and TCRγδ). Data represent at least three independent experiments.

Taken together, these data revealed that chronic stress upregulated cAMP levels and suppressed the transcriptional activity of FOXO1 in ILC3s. As a result, activation of ADRA2A signaling and suppression of VIPR2 signaling in ILC3s aggravated intestinal inflammation.

Discussion

ILC3s are required for the regulation of intestinal homeostasis. It has been reported that hyperactivation of ILC3s is closely associated with intestinal inflammation. The activation of immune cells in the intestine is modulated by the nervous system (Jakob et al., 2021). However, how gut neuronal signaling coordinates the immune response of ILC3 is largely unknown. In this study, we found that stress-elevating cAMP suppressed the expression of FOXO1. FOXO1 deficiency promoted the activation of ILC3s via upregulating expression levels of *Adra2a* and suppressing the expression of *Vipr2*. As a result, ILC3s produced large amounts of inflammatory cytokines and aggravated gut inflammation (Fig. S4).

FOXO1 is essential for the homeostasis of T cells in the intestine. Th17 is the adaptive immune counterpart of ILC3s. FOXO1 inhibits the proliferation and activation of Th17 cells (Ichiyama et al., 2016). Consistent with previous findings, we found that FOXO1 deficiency increased the cell population of Th17 cells. However, we did not observe a significant change in the cell number of ILC3s in *Foxo1*-deficient mice, indicating a different regulatory mechanism mediated by FOXO1 in ILC3s. Luu et al. found that ILC3 numbers were decreased in BM and thymus, and in contrast, NKp46$^-$ ILC3s were increased in spleen of *Foxo1,3*$^{\Delta Vav}$ mice compared with WT mice (Luu et al., 2022). By using Vav-Cre, *Foxo1* gene was depleted in all hematopoietic cells, including the progenitor cells. It is possible that the development of ILC3s was affected by *Foxo1* depletion. In addition, dysfunction of other immune cells by *Foxo1* depletion may also contribute to the altering of ILC3 function. Our results found that the frequencies and total numbers of ILC3s in small intestine and mesenteric lymph nodes did not significantly change in *Foxo1*$^{flx/flx}$*;Rorc-Cre;Rag1*$^{-/-}$ mice compared with *Foxo1*$^{+/+}$*;Rorc-Cre;Rag1*$^{-/-}$ mice. We used a more specific mouse model for the depletion of *Foxo1* in ILC3s. Moreover, deletion of FOXO1 in ILC3s of *Rag1*$^{-/-}$ mice exacerbated production of inflammatory cytokines and aggravated intestinal inflammation, indicating that FOXO1 was required to maintain ILC3 homeostasis independently of T cells. Furthermore, we found that FOXO1 regulated the function of ILC3s through a different mechanism from T cells. FOXO1 suppressed the level of *Adra2a* and promoted the expression of *Vipr2* in ILC3s. Interestingly, these two neural receptors were not expressed on Th17 cells. FOXO1 balanced the activation of ILC3s via neuroimmune regulation of these two neuronal signaling pathways. Thus, we provided new insights to distinguish the regulation of ILC3s and Th17 cells by FOXO1 in the intestine. Further studies are needed to determine how FOXO1 is differentially regulated during the development and maturation of ILC3s and Th17 cells.

The nervous and immune systems play an important role in regulating gastrointestinal diseases. ADRA2A, belonging to class A G protein–coupled receptors, plays a critical role in modulating the inflammatory processes (Leong et al., 2010). ADRA2A is reported to be associated with the development of irritable bowel syndrome and colitis (Sikander et al., 2010). Moreover, VIP, mainly expressed by enteric neurons, participates in maintaining intestinal homeostasis (Lelievre et al., 2007; Talbot et al., 2020; Zhou and Sonnenberg, 2020). Food consumption elevated the production of VIP in the intestine and inhibited the excessive production of IL-22 derived from VIPR2-expressed ILC3s, which increased lipid absorption and played a protective role in the intestinal barrier (Talbot et al., 2020). In contrast, some studies showed that VIP plays a proinflammatory role in IBD (Abad et al., 2003). Our results showed that FOXO1 suppressed the expression of ADRA2A and promoted the expression of VIPR2 in ILC3s to maintain intestinal homeostasis. The stress-associated ADRA2A signaling and diet-associated VIPR2 signaling worked in concert to regulate the function of ILC3s, indicating that stress and diet signaling balanced intestinal homeostasis. Activation of ADRA2A signaling by stress and suppression of VIPR2 signaling by fasting might be risk factors for colitis.

Chronic restraint stress is an early trigger for anxiety and depression disorder (de Kloet et al., 2005). Several studies showed that stress impaired the function of the digestive system and caused IBD bidirectionally (Gao et al., 2018; Sun et al., 2019). Chronic stress induces intestinal inflammation by disrupting gut barrier and hence promoting inflammatory cell infiltration and microbiota disturbance (Zheng et al., 2009). We found that the chronic restraint stress promoted hyperactivation of ILC3s and induced colitis via the cAMP–FOXO1 axis. Elevation of cAMP downregulated FOXO1 level, accompanied by an increased level of ADRA2A and downregulation of VIPR2 expression in ILC3s. The connection between neuronal signaling pathways and immune regulation mediated by FOXO1 might be exploitable in the therapies for stress-related intestinal disorders.

In summary, we revealed that cAMP–FOXO1 signaling balanced intestinal homeostasis via neuronal signaling in ILC3s. Our study showed a regulatory circuit between the immune system and the nervous system in the maintenance of gut homeostasis, which might provide potential targets for treating intestinal inflammation.

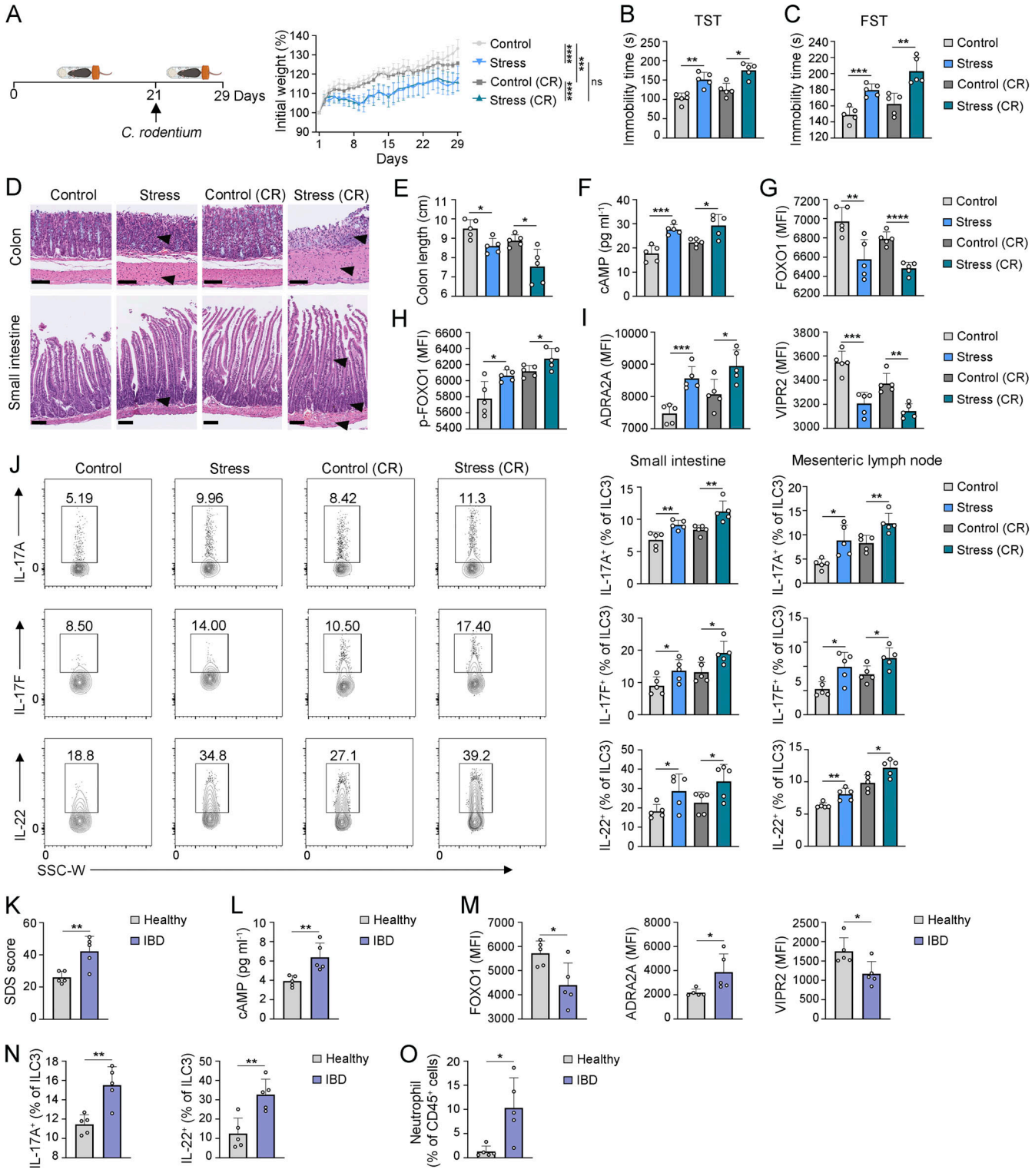

Figure 6. **Chronic stress induces hyperactivation of ILC3s and intestinal inflammation. (A)** Schematic strategy of the experimental setup of stressed mouse models (left). WT mice were placed in 50-ml conical centrifuge tubes with ventilation holes for 4 h per day for 21 d followed by CR infection according to a previous study (Li et al., 2020). Body weight changes of control and stressed mice with or without CR infection were measured daily and calculated as means ± SD. ns, not significantly; ***, P < 0.001, ****, P < 0.0001, by two-way ANOVA. *n* = 5 for each group. **(B and C)** Immobility time of control and stressed mice with or without CR infection were analyzed in tail suspension test (TST; B) and forced swimming test (FST; C). The immobility time was analyzed and shown as means ± SD. *, P < 0.05, **, P < 0.01, ***, P < 0.001, by two-tailed unpaired Student's *t* test. *n* = 5 for each group. **(D)** Representative H&E staining of the colon and small intestine sections from control and stressed mice with or without CR infection. The arrowheads indicated the inflammatory lesions. Scale bars, 100 µm. **(E)** Colon lengths of control and stressed mice with or without CR infection were measured and shown as means ± SD. *, P < 0.05, by two-tailed unpaired Student's *t* test. *n* = 5 for each group. **(F)** Serum cAMP concentrations of control and stressed mice with or without CR infection were examined by ELISA and

shown as means ± SD. *, P < 0.05, ***, P < 0.01, by two-tailed unpaired Student's *t* test. *n* = 5 for each group. **(G and H)** Expression levels of FOXO1 and phosphorylated p-FOXO1 in ILC3s from control or stressed mice with or without CR infection were analyzed by flow cytometry. MFI of FOXO1 (G) and p-FOXO1 (H) are shown as means ± SD. *, P < 0.05, **, P < 0.01, ****, P < 0.0001, by two-tailed unpaired Student's *t* test. *n* = 5 for each group. **(I)** Expression of ADRA2A and VIPR2 on ILC3s of control or stressed mice with or without CR infection were analyzed by flow cytometry and shown as means ± SD. *, P < 0.05, **, P < 0.01, ***, P < 0.001, by two-tailed unpaired Student's *t* test. *n* = 5 for each group. **(J)** The proportion of IL-17A–, IL-17F–, and IL-22–positive ILC3s in the small intestine and mesenteric lymph nodes from control and stressed mice with or without CR infection were analyzed by flow cytometry and shown as means ± SD. The representative flow cytometry plots of intestinal ILC3s are shown on the left panel. *, P < 0.05, **, P < 0.01, by two-tailed unpaired Student's *t* test. *n* = 5 for each group. **(K)** Self-rating depression scale (SDS) scores of healthy donors and IBD patients were evaluated and shown as means ± SD. **, P < 0.01, by two-tailed unpaired Student's *t* test. *n* = 5 for each group. **(L)** Serum cAMP levels in IBD patients were measured by ELISA and shown as means ± SD. **, P < 0.01, by two-tailed unpaired Student's *t* test. *n* = 5 for each group. **(M)** Expression of FOXO1, ADRA2A, and VIPR2 in ILC3s from the intestine of healthy donors and IBD patients were analyzed by flow cytometry. MFI of indicated proteins was shown as means ± SD. *, P < 0.05, by two-tailed unpaired Student's *t* test. *n* = 5 for each group. **(N)** The proportion of IL-17A$^+$, IL-22$^+$ ILC3s in the intestine from healthy participants and IBD patients were analyzed by flow cytometry and shown as means ± SD. **, P < 0.01, by two-tailed unpaired Student's *t* test. *n* = 5 for each group. **(O)** The proportion of neutrophils in the intestine from healthy participants and IBD patients were analyzed by flow cytometry and shown as means ± SD. *, P < 0.05, by two-tailed unpaired Student's *t* test. *n* = 5 for each group. Gate strategy for mouse ILC3 analysis was Lin$^-$NK1.1$^-$KLRG1$^-$CD45$^+$CD127$^+$RORγt$^+$ (Lin = CD3, CD19, CD11b, CD11c, Gr-1, TER-119, TCRβ, TCRγδ). Gate strategy for human ILC3 analysis was Lin$^-$CD45$^+$CD127$^+$CD117$^+$ (Lin = CD3, CD14, CD19, CD20, CD56). Data represent at least three independent experiments.

Materials and methods

Antibodies and reagents

Anti-mouse CD3 (17A2), anti-mouse CD19 (eBio1D3), anti-mouse NK1.1 (PK136), anti-mouse KLRG1 (2F1), anti-mouse CD45.2 (104), and anti-mouse CD127 (SB/199) were purchased from eBioscience; anti-mouse TCRβ (H57-597), anti-mouse TCRγδ (GL3), anti-mouse TER-119 (TER-119), anti-mouse Gr-1 (RB6-8C5), anti-mouse CD11b (M1/70), anti-mouse CD11c (N418), anti-mouse CD90.2 (30-H12), anti-mouse IL-17A (TC11-18H10.1), anti-mouse IL-17F (9D3.1C8), anti-mouse IL-22 (Poly5164), anti-human Lineage (CD3/14/19/20/56; UCHT1/HCD14/HIB19/2H7/HCD56), anti-human CD45 (2D1), anti-human CD117 (104D2), anti-human CD127 (IL-7Rα), and anti-GFP (FM264G) were purchased from BioLegend; anti-mouse RORγt (Q31-378) was purchased from BD Bioscience; anti-ADRA2A (NB100-2819) was purchased from Novus Biologicals; anti-VIPR2/VPAC2 (SP235) and anti-VIP (EPR23288-43) were purchased from Abcam; anti-FOXO1 (2880) and anti-phospho-FOXO1 (9464) were purchased from Cell Signaling Technology. Goat anti-rat IgG (H+L) and goat anti-rabbit IgG (H+L) were purchased from Invitrogen. Recombinant murine IL-7 was purchased from PeproTech; recombinant murine IL-23 was purchased from R&D. Brefeldin A was purchased from eBioscience. PMA, ionomycin, N6,2′-O-dibutyryladenosine 3′,5′-cyclic monophosphate sodium salt (cAMP; D0260), and clonidine hydrochloride (C7897) were purchased from Sigma. Yohimbine HCl (V1127) was purchased from InvivoChem. BAY 55-9837 (2711) was purchased from Tocris. PG99-465 (Myristoyl-(Lys$^{12.27.28}$)-VIP-Gly-Gly-Thr [free acid]) was purchased from Bachem.

Mice

C57BL/6 mice (male and female) were obtained from Beijing Vital River Laboratory Animal Technology. *Foxo1*$^{flx/flx}$ mice were kind gifts from Dr. Ming Li (Memorial Sloan-Kettering Cancer Center, New York, NY, USA; Ouyang et al., 2012). *Adra2a*$^{flx/flx}$ mice were generated by Cyagen Bioscience. *Rorc*^{cre} mice were purchased from the Jackson Laboratory. *Rag1*$^{-/-}$ mice were from GemPharmatech Co., Ltd. RORγt-GFP mice were kind gifts from Dr. Xiaohuan Guo. All transgenic mice were bred and maintained in the animal facility of the Institute of Microbiology, Chinese Academy of Sciences (IMCAS) in specific pathogen–free conditions. Age- and sex-matched littermates between 8 and 16 wk of age were used in all experiments. Both male and female mice were used in experiments. Mice were assigned randomly to experimental groups. All animal protocols were approved by Animal Ethics Committee in IMCAS and conducted in compliance with the recommendations in the Guide for the Care and Use of Laboratory Animals of the IMCAS Ethics Committee.

Participants

All experiments involving human samples were approved by the Medical Ethics Committee of the IMCAS and Seventh Medical Center of Chinese PLA General Hospital. All human participants provided informed consent. Healthy volunteers and patients with CD or UC were recruited from Seventh Medical Center of Chinese PLA General Hospital. The diagnosis of CD and UC was based on clinical symptoms, endoscopic examination, and histological scores, and the disease severity was tested based on CD activity index or Mayo scores for UC. All patients were invited to report their stress symptoms by means of an adapted version of the self-rating anxiety scale for stress. The intestinal biopsies were taken from participants undergoing routine endoscopy and peripheral blood was collected with procoagulant tubes for further analysis.

Preparation of mouse tissue samples and flow cytometry

Euthanasia was by CO_2 inhalation followed by cervical dislocation. The intestines from euthanized mice were removed from mesenteric fat tissue and washed in ice-cold PBS. Peyer's patches were identified and removed. Next, intestines were opened longitudinally and subsequently cleaned in cold PBS to remove fecal contents. Then, intestines were cut into pieces and epithelial cells were removed by three times 20-min incubation on a horizontal shaker with digestion buffer I (5 mM EDTA Ca^{2+} and Mg^{2+} free Hank's medium) at 37°C. After each washing step, tissue was vortexed and the epithelial fraction discarded. Then, remaining tissue was cut into fine pieces and digested by two 40-min incubations on a horizontal shaker with digestion buffer II containing 10% FBS, Collagenase II and III (1 mg ml^{-1}; Worthington), DNase I (200 µg ml^{-1}; Roche), and dispase (4 U ml^{-1}; Sigma-Aldrich) at 37°C. After each digestion, cells were harvested and filtered through a 70-µm cell strainer. Purified cells were washed and resuspended in PBS supplemented with FBS

(0.5%) and stained for flow cytometry analysis or sorting. Mesenteric lymph nodes were mechanically disrupted and passed through 70-μm cell strainer for single-cell suspension harvest.

Single-cell suspensions were labeled for flow cytometry analysis using fluorophore-conjugated antibodies for 40 min on ice. For intracellular staining, cells were fixed and permeabilized using a Foxp3/Transcription Factor Staining Buffer Set (eBioscience). Then, cells were incubated with intracellular antibodies for 50 min on ice. FACS data were acquired using BD FACSCanto II (BD Biosciences) or BD FACSAria III (BD Biosciences), and analysis was carried out using FlowJo software (V.10.0.8; Tree Star).

The following antibodies were used to label the ILC3s for sorting of flow cytometry: Lin (CD3, CD19, TCRβ, TCRγδ, TER-119, Gr-1, CD11b, CD11c)$^-$NK1.1$^-$KLRG1$^-$CD45^{low}CD90.2^{hi}CD127$^+$. The following antibodies were used for ILC3s analysis of flow cytometry: Lin (CD3, CD19, TCRβ, TCRγδ, TER-119, Gr-1, CD11b, CD11c)$^-$NK1.1$^-$KLRG1$^-$CD45$^+$CD127$^+$RORγt$^+$. For inflammatory cytokine (IL-17A, IL-17F, and IL-22) staining, cells were re-stimulated in completed RPMI1640 media with PMA (50 ng ml^{-1}; Sigma-Aldrich), ionomycin (1 μM; Sigma-Aldrich), and Brefeldin A (eBioscience) at 37°C, 5% CO_2 for 4 h before staining.

Human intestinal samples and flow cytometry

Single-cell suspensions from human intestinal tissues were obtained by incubating tissues on a horizontal shaker with digestion buffer I (5 mM EDTA Ca^{2+} and Mg^{2+} free Hank's medium) at 37°C for 30 min to remove the epithelial layer. Tissues were then cut into small pieces and incubated in the same way as the murine intestine cells harvest method. For flow cytometry, human ILC3s were stained with antibodies according to the following panel: Lin$^-$CD45$^+$CD127$^+$CD117$^+$ (Lin = CD3, CD14, CD19, CD20, CD56).

Infection of CR

CR (DBS100, ATCC 51459) was cultured overnight in Luria-Bertani broth medium at 37°C, orbital shaking at 180 rpm. After 16 h, the bacteria were centrifuged, the supernatant was discarded, and the pellet was resuspended in sterile PBS. Mice were infected with 2 × 10^9 colony-forming units (CFU) of CR in 200 μl PBS via oral gavage. CR quantification was measured by plating bacteria in serial dilutions on MacConkey agar plates overnight at 37°C. Mice were sacrificed on day 8 after infection.

Enzyme-linked immunosorbent assays (ELISA)

Concentrations of IL-17A and IL-22 in mice serum and cell culture supernatants were determined using ELISA MAX Deluxe Set Mouse IL-17A (432504; BioLegend) and ELISA MAX Deluxe Set Mouse IL-22 (436304; BioLegend) according to the manufacturer's instructions. Quantification of the cAMP concentration was done using Cyclic AMP XP Assay Kit (4339S; Cell Signaling Technology).

RNA extraction and RT-qPCR analysis

Total RNA was extracted using TRIZOL (Invitrogen) and reverse transcribed using FastKing RT Kit (With gDNase; KR116; Tiangen). RT-qPCR analysis was performed with the SuperReal PreMix Plus (SYBR Green; FP205; Tiangen) on an Applied Biosystems QuantStudio 7 machine according to the manufacturer's instructions. Expression data were normalized to the expression of housekeeping gene *Gapdh* (reference gene). The following primer sequences were used: *Gapdh*: 5′-AGGTCGGTGTGAACG GATTTG-3′ (forward) and 5′-TGTAGACCATGTAGTTGAGGTCA-3′ (reverse); *Adra2a*: 5′-GTGACACTGACGCTGGTTTG-3′ (forward) and 5′-CCAGTAACCCATAACCTCGTTG-3′ (reverse); *Vipr2*: 5′-GAC CTGCTACTGCTGGTTG-3′ (forward) and 5′-CAGCTCTGCACATTT TGTCTCT-3′ (reverse); *Foxo1*: 5′-CCCAGGCCGGAGTTTAACC-3′ (forward) and 5′-GTTGCTCATAAAGTCGGTGCT-3′ (reverse). All primer sequences were determined using PrimerBank, a public resource for PCR primers.

Imaging flow cytometry

To visualize intracellular localization of FOXO1 protein, ILCs in small intestine from WT mice were isolated using MojoSort Mouse Hematopoietic Progenitor Cell Isolation Kit (480003; BioLegend) and cultured in RPMI1640 complete medium supplemented with 10% FBS, 1× penicillin-streptomycin, 2 mM glutamine, 25 ng ml^{-1} IL-7 (PeproTech), 25 ng ml^{-1} IL-23 (R&D), and vehicle or cAMP (50 μM) for 16 h. ILCs were stained with PI, FOXO1, Lin (CD3, CD19, CD11b, CD11c, Gr-1, TER-119, TCRβ, TCRγδ, NK1.1), CD45, and RORγt, and analyzed by imaging flow cytometry (Amnis ImageStream MarkII; Merck). The nuclear localization of FOXO1 was analyzed using the IDEAS software v.6.2 (Merck).

ILC3 isolation and in vitro stimulation

ILC3s were isolated from small intestine of WT mice using flow cytometry (ILC3 = Lin$^-$NK1.1$^-$KLRG1$^-$CD45^{low}CD90^{hi}CD127$^+$, Lin = CD3, CD19, TCRβ, TCRγδ, TER-119, Gr-1, CD11b, and CD11c). For in vitro experiments of cytokines secretion, 5 × 10^4 ILC3s were cultured per well in a 96-well round bottom plate in RPMI1640 complete medium supplemented with 10% FBS, 1× penicillin-streptomycin, 2 mM glutamine. ILC3s were stimulated with 25 ng ml^{-1} IL-7 (PeproTech), 25 ng ml^{-1} IL-23 (R&D), and vehicle or cAMP with indicated concentrations. The supernatants were collected for ELISA, and the cell pellets were measured by flow cytometry for IL-17A$^+$, IL-17F$^+$, and IL-22$^+$ ILC3s.

Histopathology analysis

Mouse colon and small intestine tissues were prepared in the Swiss roll technique, fixed with 4% paraformaldehyde, and embedded in paraffin. Serial 5-μm sections were stained with hematoxylin and eosin (H&E). The arrowheads indicated the inflammatory lesions with swollen and infiltration of immune cells.

Immunofluorescence staining and confocal microscopy

Mouse small intestine tissues were prepared in the Swiss roll technique, fixed in 4% paraformaldehyde overnight, and dehydrated in 30% sucrose overnight at 4°C. Dehydrated small intestine tissues were embedded in optimal cutting temperature compound medium (Tissue-Tek) and stored at −80°C until sectioning at a thickness of 8 μm using a cryotome (Leica). Frozen slides were retrieved at room temperature and excess optimal

cutting temperature compound medium was removed in PBS before blocking in PBS with 10% normal goat serum and 0.3% Triton X-100 for 30 min. Tissue sections were then stained with the following primary antibodies diluted in blocking buffer overnight at 4°C: anti-GFP 1:100 and anti-VIP 1:500. Sections were washed three times with PBST (PBS + 0.05% Tween-20) and then incubated with secondary antibodies (anti-rat IgG-594 and anti-rabbit IgG-488) diluted 1:500 in blocking buffer for 1 h at room temperature. Tissue sections were then washed three times in PBST and incubated with anti-mouse CD3 (17A2) diluted 1:500 in blocking buffer for 2 h at room temperature. Tissue sections were then washed three times in PBST, incubated with DAPI (Sigma-Aldrich) for 3 min before a final wash in PBS, and mounted with antifade regent. Stained sections were imaged on a confocal microscope (Leica SP8).

scRNA-seq and data processing

10x Genomics scRNA-seq was performed as previously described (Ma et al., 2023). Briefly, we isolated mouse intestinal $CD3^+$ cells ($Lin^-CD45.2^+CD3^+$, Lin = CD19, CD11b, CD11c, TER-119, Gr-1) and ILC3s ($Lin^-CD3^-CD45^{low}CD127^+CD90^{hi}$). Sorted cells were encapsulated into droplets, and libraries were prepared using Chromium Single Cell 3′ Regent Kit V3.1 according to the manufacturer's protocol (10x Genomics). scRNA-seq libraries were sequenced on an Illumina Novaseq 6000. Reads were processed by CellRanger software (10x Genomics) using the mm10 reference genome. According to the flow cytometry analysis, the same mouse strains have similar lymphocyte distributions. Therefore, we pooled ILC3s and $CD3^+$ T cells from three mice of the same mouse strain together as one sample for scRNA-seq per experimental condition. One scRNA-seq experiment was run for each sample.

Downstream analysis was performed with Seurat v.4.1.2. We further filtered out low-quality cells and cell doublets with <200 genes detected, >5,000 genes detected, or >10% mitochondrial reads. Normalization was performed with Seurat (v.4.1.2) and integrated by canonical correlation analysis. The graph representing cells with similar expression patterns was generated with the FindNeighbors function using the 20 largest principal components. Cell clusters were generated using the Louvain algorithm implemented by the FindClusters function with the resolution parameter equal to 0.9. Marker genes for each cluster were determined using the Wilcoxon test on the raw counts, implemented by the function FindAllMarkers, and included only positive marker genes with log-fold changes >0.25 and Bonferroni-corrected P values <0.01. Dimensionality reduction by t-distributed stochastic neighbor embedding was performed using the RuntSNE function with the 20 largest principal components. All visualizations of scRNA-seq data were generated using the Seurat package as well as ggplot2 version 4.1.2.

Chronic restraint stress (CRS)

The CRS procedure was performed based on previous studies (Li et al., 2020). In brief, the C57BL/6J mice were placed in 50 ml conical centrifuge tubes with ventilation holes for 4 h (10:00 am–2:00 pm) per day for 29 d. A hole was created in the center of the lid to allow the tail of the mouse to pass through. The stress (CR) group mice were infected 2×10^9 CR via oral gavage on day 21 of CRS treatment and sacrificed on day 8 after CR infection. Mice were not allowed forward and backward movement, were not physically compressed, and did not experience pain.

Forced swimming test

Mice were placed individually in a 3-liter glass chamber filled with 15 cm of water (temperature 25 ± 1°C) for 6 min. The lengths of periods of immobility or struggling during the 6-min test period were measured. Water was replaced between every test. Following swim sessions, mice were removed from the cylinder, dried with a towel, and returned to their home cages.

Tail suspension test

Mice were individually suspended by the distal portion of their tails using adhesive tape, keeping their head 15 cm from the table. The test sessions lasted 6 min, and the immobility time was determined by a skilled observer. The mice were regarded as immobile only when they hung passively and fully motionless.

FOXO1 CUT&Tag assay

FOXO1 genome-wide binding regions in ILC3s were detected by CUT&Tag assay using Hyperactive In-Situ ChIP Library Prep Kit for Illumina (TD901; Vazyme Biotech Co., Ltd) according to the manufacturer's recommendation. Briefly, ConA Beads (10 µl per sample) were washed with ConA Binding Buffer. 1×10^5 ILC3s were isolated and washed with wash buffer. The cells were mixed with ConA beads and incubated with anti-FOXO1 (Abcam) or anti-IgG overnight at 4°C. Goat anti-rabbit IgG antibody was added into the sample and incubated for 1 h at room temperature. After washing away the unbounded secondary antibody, 0.04 µM Transposon was added and incubated with cells for 1 h at room temperature. The sample was washed by Dig-300 buffer and followed with incubation by Tagmentation Buffer for 1 h. Next, DNA was isolated and amplified with P5 and P7 primers and purified for high-throughput sequencing. Paired-end sequencing was carried out with the Illumina NovaSeq 6000 with read length of 150 bp. Paired-end reads were aligned using Bowtie2. The peak visualization in genome was shown by IGV software.

ChIP-qPCR assays

1×10^5 ILC3s from small intestine of WT mice were analyzed by FOXO1 CHIP-qPCR using ChIP-IT High Sensitivity kit (53040; Active Motif) according to the manufacturer's instruction. Anti-FOXO1 (39670; Abcam) was used for immunoprecipitation. Primers used for ChIP-qPCR were as follows: *Adra2a*-N: 5′-CGTGATCTTCCTGCTGCTCGTC-3′ (forward) and 5′-GCTTGGCAGTAGATGGCAAGGT-3′ (reverse); *Adra2a*-B1: 5′-GGGACAGACAGCCATCTTGGTT-3′ (forward) and 5′-GCACCTTTACCCTGCAACCCTT-3′ (reverse); *Adra2a*-B2: 5′-TGTCATGGCGCTCTTCATAAAG-3′ (forward) and 5′-CTCTCTGCTTGCCTGGCTTT-3′ (reverse); *Vipr2*-N: 5′-GGCACAACACAAGGCTGAACTC-3′ (forward) and 5′-GGTGACTGCTTGGTTCTGATGG-3′ (reverse); *Vipr2*-B1: 5′-GCTGCTGCTGCTTTGGGTATGA-3′ (forward) and 5′-TCCTGGCA

CCTTCCACTTGAGT-3′ (reverse); *Vipr2*-B2: 5′-ACCTTCGCTCCT CCAGGATACC-3′ (forward) and 5′-CCAGGGTTCCAACCACAG CAAT-3′ (reverse).

Luciferase reporter assays

All reporter assays were performed by co-transfection of HEK293T cells with pcDNA4-FOXO1 and pGL3 vectors containing different regions of the mouse *Adra2a* promoter or *Vipr2* promoter. Firefly and Renilla luciferase actives were measured by the Dual-Luciferase Reporter Assay System (E2920; Promega). Data were normalized to the activity of Renilla luciferase. Cell line HEK293T was tested negative for mycoplasma contamination.

Statistical analysis

Statistical analysis was performed using GraphPad Prism v9. All statistical graphs represented the mean ± SD and were determined by unpaired two-tailed Student's *t* test, one-way ANOVA, and two-way ANOVA according to the type of experiments. The statistical significances of differences (*, $P < 0.05$, **, $P < 0.01$, ***, $P < 0.001$, ****, $P < 0.0001$) are specified throughout the figures and legends. All flow cytometry data were analyzed with FlowJo (Treestar). No statistical methods were used to predetermine sample sizes.

Online supplemental material

Fig. S1 shows that FOXO1 deficiency in ILC3s and Th17 cells results in intestinal inflammation. Fig. S2 shows that FOXO1 suppresses the expression of inflammatory cytokines in ILC3s. Fig. S3 shows that FOXO1 regulates ADRA2A and VIPR2 signaling in ILC3s. Fig. S4 demonstrates the work model for FOXO1-induced neuronal signaling regulation of ILC3s in the intestine. Table S1 shows the quality control metrics of scRNA-seq data. Table S2 shows the colitis-related gene set.

Data availability

The scRNA-seq and CUT&Tag data generated in this study have been deposited in the Genome Sequence Archive (GSA) of the National Genomics Data Center, China National Center for Bioinformation database under accession code CRA011143 and CRA011145. All other relevant data are available from the corresponding author upon reasonable request.

Acknowledgments

We thank Dr. Ming Li (Memorial Sloan-Kettering Cancer Center, USA) for providing *Foxo1*$^{flx/flx}$ mice. We thank Dr. Xiaohuan Guo (Tsinghua University, Beijing, China) for providing RORγt-GFP mice. We thank Dr. Mingzhao Zhu (Institute of Biophysics, Chinese Academy of Sciences, Beijing, China) for providing CR. We thank Dr. Pengyan Xia (Peking University, Beijing, China) for technical support. We thank Tong Zhao (Institute of Microbiology, Chinese Academy of Sciences, Beijing, China) for technical support. Cartoons in Fig. 6 A and Fig. S4 and graphical abstract were created with BioRender.com.

This work was supported by the National Key R&D Program of China (2021YFA1300202, 2022YFC2302900, 2020YFA0803501), the National Natural Science Foundation of China (92169113, 31930036, 81921003), Key Research Program of Frontier Sciences of Chinese Academy of Sciences (ZDBS-LY-SM025), CAS Project for Young Scientists in Basic Research (YSBR-010), and Youth Innovation Promotion Association of CAS to S. Wang.

Author contributions: F. Shao performed experiments, analyzed data, and wrote the paper; Z. Liu performed experiments and analyzed data; Q. Wei provided IBD tissue samples and analyzed data; D. Yu, M. Zhao, X. Zhang, and X. Gao performed experiments. Z. Fan provided mouse models. S. Wang initiated and organized the study, and organized, designed, and wrote the paper.

Disclosures: The authors declare no competing interests exist.

Submitted: 21 January 2023
Revised: 30 May 2023
Accepted: 20 July 2023

References

Abad, C., C. Martinez, M.G. Juarranz, A. Arranz, J. Leceta, M. Delgado, and R.P. Gomariz. 2003. Therapeutic effects of vasoactive intestinal peptide in the trinitrobenzene sulfonic acid mice model of Crohn's disease. *Gastroenterology*. 124:961–971. https://doi.org/10.1053/gast.2003.50141

Ahrends, T., B. Aydin, F. Matheis, C.H. Classon, F. Marchildon, G.C. Furtado, S.A. Lira, and D. Mucida. 2021. Enteric pathogens induce tissue tolerance and prevent neuronal loss from subsequent infections. *Cell*. 184: 5715–5727.e12. https://doi.org/10.1016/j.cell.2021.10.004

Anton, S.E., C. Kayser, I. Maiellaro, K. Nemec, J. Möller, A. Koschinski, M. Zaccolo, P. Annibale, M. Falcke, M.J. Lohse, and A. Bock. 2022. Receptor-associated independent cAMP nanodomains mediate spatiotemporal specificity of GPCR signaling. *Cell*. 185:1130–1142.e11. https://doi.org/10.1016/j.cell.2022.02.011

Bisgaard, T.H., K.H. Allin, L. Keefer, A.N. Ananthakrishnan, and T. Jess. 2022. Depression and anxiety in inflammatory bowel disease: Epidemiology, mechanisms and treatment. *Nat. Rev. Gastroenterol. Hepatol.* 19:717–726. https://doi.org/10.1038/s41575-022-00634-6

Chung, S., J.Y. Kim, M.A. Song, G.Y. Park, Y.G. Lee, M. Karpurapu, J.A. Englert, M.N. Ballinger, N. Pabla, H.Y. Chung, and J.W. Christman. 2019. FoxO1 is a critical regulator of M2-like macrophage activation in allergic asthma. *Allergy*. 74:535–548. https://doi.org/10.1111/all.13626

Conlin, V.S., X. Wu, C. Nguyen, C. Dai, B.A. Vallance, A.M. Buchan, L. Boyer, and K. Jacobson. 2009. Vasoactive intestinal peptide ameliorates intestinal barrier disruption associated with Citrobacter rodentium-induced colitis. *Am. J. Physiol. Gastrointest. Liver Physiol.* 297:G735–G750. https://doi.org/10.1152/ajpgi.90551.2008

Daitoku, H., M. Hatta, H. Matsuzaki, S. Aratani, T. Ohshima, M. Miyagishi, T. Nakajima, and A. Fukamizu. 2004. Silent information regulator 2 potentiates Foxo1-mediated transcription through its deacetylase activity. *Proc. Natl. Acad. Sci. USA*. 101:10042–10047. https://doi.org/10.1073/pnas.0400593101

de Kloet, E.R., M. Joëls, and F. Holsboer. 2005. Stress and the brain: From adaptation to disease. *Nat. Rev. Neurosci.* 6:463–475. https://doi.org/10.1038/nrn1683

Delpoux, A., N. Marcel, R. Hess Michelini, C.D. Katayama, K.A. Allison, C.K. Glass, S.M. Quiñones-Parra, C. Murre, L. Loh, K. Kedzierska, et al. 2021. FOXO1 constrains activation and regulates senescence in CD8 T cells. *Cell Rep.* 34:108674. https://doi.org/10.1016/j.celrep.2020.108674

Dominguez-Sola, D., J. Kung, A.B. Holmes, V.A. Wells, T. Mo, K. Basso, and R. Dalla-Favera. 2015. The FOXO1 transcription factor instructs the germinal center dark zone Program. *Immunity*. 43:1064–1074. https://doi.org/10.1016/j.immuni.2015.10.015

Gao, X., Q. Cao, Y. Cheng, D. Zhao, Z. Wang, H. Yang, Q. Wu, L. You, Y. Wang, Y. Lin, et al. 2018. Chronic stress promotes colitis by disturbing the gut microbiota and triggering immune system response. *Proc. Natl. Acad. Sci. USA*. 115:E2960–E2969. https://doi.org/10.1073/pnas.1720696115

Geremia, A., C.V. Arancibia-Cárcamo, M.P. Fleming, N. Rust, B. Singh, N.J. Mortensen, S.P. Travis, and F. Powrie. 2011. IL-23-responsive innate

lymphoid cells are increased in inflammatory bowel disease. *J. Exp. Med.* 208:1127–1133. https://doi.org/10.1084/jem.20101712
Godinho-Silva, C., F. Cardoso, and H. Veiga-Fernandes. 2019. Neuro-immune cell units: A new paradigm in physiology. *Annu. Rev. Immunol.* 37:19–46. https://doi.org/10.1146/annurev-immunol-042718-041812
Gronke, K., P.P. Hernández, J. Zimmermann, C.S.N. Klose, M. Kofoed-Branzk, F. Guendel, M. Witkowski, C. Tizian, L. Amann, F. Schumacher, et al. 2019. Interleukin-22 protects intestinal stem cells against genotoxic stress. *Nature*. 566:249–253. https://doi.org/10.1038/s41586-019-0899-7
Hedrick, S.M., R. Hess Michelini, A.L. Doedens, A.W. Goldrath, and E.L. Stone. 2012. FOXO transcription factors throughout T cell biology. *Nat. Rev. Immunol.* 12:649–661. https://doi.org/10.1038/nri3278
Hernandez, J.B., C. Chang, M. LeBlanc, D. Grimm, J. Le Lay, K.H. Kaestner, Y. Zheng, and M. Montminy. 2015. The CREB/CRTC2 pathway modulates autoimmune disease by promoting Th17 differentiation. *Nat. Commun.* 6:7216. https://doi.org/10.1038/ncomms8216
Ichiyama, K., A. Gonzalez-Martin, B.S. Kim, H.Y. Jin, W. Jin, W. Xu, M. Sabouri-Ghomi, S. Xu, P. Zheng, C. Xiao, and C. Dong. 2016. The microRNA-183-96-182 cluster promotes T helper 17 cell pathogenicity by negatively regulating transcription factor Foxo1 expression. *Immunity*. 44:1284–1298. https://doi.org/10.1016/j.immuni.2016.05.015
Jacobson, A., D. Yang, M. Vella, and I.M. Chiu. 2021. The intestinal neuro-immune axis: Crosstalk between neurons, immune cells, and microbes. *Mucosal Immunol.* 14:555–565. https://doi.org/10.1038/s41385-020-00368-1
Jakob, M.O., M. Kofoed-Branzk, D. Deshpande, S. Murugan, and C.S.N. Klose. 2021. An integrated view on neuronal subsets in the peripheral nervous system and their role in immunoregulation. *Front. Immunol.* 12:679055. https://doi.org/10.3389/fimmu.2021.679055
Jarade, A., J.P. Di Santo, and N. Serafini. 2021. Group 3 innate lymphoid cells mediate host defense against attaching and effacing pathogens. *Curr. Opin. Microbiol.* 63:83–91. https://doi.org/10.1016/j.mib.2021.06.005
Jarret, A., R. Jackson, C. Duizer, M.E. Healy, J. Zhao, J.M. Rone, P. Bielecki, E. Sefik, M. Roulis, T. Rice, et al. 2020. Enteric nervous system-derived IL-18 orchestrates mucosal barrier immunity. *Cell*. 180:50–63.e12. https://doi.org/10.1016/j.cell.2019.12.016
Kibbe, W.A., C. Arze, V. Felix, E. Mitraka, E. Bolton, G. Fu, C.J. Mungall, J.X. Binder, J. Malone, D. Vasant, et al. 2015. Disease ontology 2015 update: An expanded and updated database of human diseases for linking biomedical knowledge through disease data. *Nucleic Acids Res.* 43: D1071–D1078. https://doi.org/10.1093/nar/gku1011
Laarakker, M.C., J.R. Raai, H.A. van Lith, and F. Ohl. 2010. The role of the alpha 2A-adrenoceptor in mouse stress-coping behaviour. *Psychoneuroendocrinology*. 35:490–502. https://doi.org/10.1016/j.psyneuen.2009.08.014
Lee, E.H., J.Y. Park, H.J. Kwon, and P.L. Han. 2021. Repeated exposure with short-term behavioral stress resolves pre-existing stress-induced depressive-like behavior in mice. *Nat. Commun.* 12:6682. https://doi.org/10.1038/s41467-021-26968-4
Lee, J.S., M. Cella, K.G. McDonald, C. Garlanda, G.D. Kennedy, M. Nukaya, A. Mantovani, R. Kopan, C.A. Bradfield, R.D. Newberry, and M. Colonna. 2011. AHR drives the development of gut ILC22 cells and postnatal lymphoid tissues via pathways dependent on and independent of Notch. *Nat. Immunol.* 13:144–151. https://doi.org/10.1038/ni.2187
Lelievre, V., G. Favrais, C. Abad, H. Adle-Biassette, Y. Lu, P.M. Germano, G. Cheung-Lau, J.R. Pisegna, P. Gressens, G. Lawson, and J.A. Waschek. 2007. Gastrointestinal dysfunction in mice with a targeted mutation in the gene encoding vasoactive intestinal polypeptide: A model for the study of intestinal ileus and hirschsprung's disease. *Peptides*. 28: 1688–1699. https://doi.org/10.1016/j.peptides.2007.05.006
Leong, J., M. Zhou, A. Jacob, and P. Wang. 2010. Aging-related hyperinflammation in endotoxemia is mediated by the alpha2A-adrenoceptor and CD14/TLR4 pathways. *Life Sci.* 86:740–746. https://doi.org/10.1016/j.lfs.2010.03.009
Li, J., L. Sha, and Q. Xu. 2020. An early increase in glutamate is critical for the development of depression-like behavior in a chronic restraint stress (CRS) model. *Brain Res. Bull.* 162:59–66. https://doi.org/10.1016/j.brainresbull.2020.05.013
Li, X., F. Murray, N. Koide, J. Goldstone, S.M. Dann, J. Chen, S. Bertin, G. Fu, L.S. Weinstein, M. Chen, et al. 2012. Divergent requirement for Gαs and cAMP in the differentiation and inflammatory profile of distinct mouse Th subsets. *J. Clin. Invest.* 122:963–973. https://doi.org/10.1172/JCI59097
Li, Z., R. Ma, S. Ma, L. Tian, T. Lu, J. Zhang, B.L. Mundy-Bosse, B. Zhang, G. Marcucci, M.A. Caligiuri, and J. Yu. 2022. ILC1s control leukemia stem cell fate and limit development of AML. *Nat. Immunol.* 23:718–730. https://doi.org/10.1038/s41590-022-01198-y
Liu, S., L. Lai, Q. Zuo, F. Dai, L. Wu, Y. Wang, Q. Zhou, J. Liu, J. Liu, L. Li, et al. 2014. PKA turnover by the REGγ-proteasome modulates FoxO1 cellular activity and VEGF-induced angiogenesis. *J. Mol. Cell. Cardiol.* 72:28–38. https://doi.org/10.1016/j.yjmcc.2014.02.007
Longman, R.S., G.E. Diehl, D.A. Victorio, J.R. Huh, C. Galan, E.R. Miraldi, A. Swaminath, R. Bonneau, E.J. Scherl, and D.R. Littman. 2014. CX_3CR1^+ mononuclear phagocytes support colitis-associated innate lymphoid cell production of IL-22. *J. Exp. Med.* 211:1571–1583. https://doi.org/10.1084/jem.20140678
Lorton, D., and D.L. Bellinger. 2015. Molecular mechanisms underlying β-adrenergic receptor-mediated cross-talk between sympathetic neurons and immune cells. *Int. J. Mol. Sci.* 16:5635–5665. https://doi.org/10.3390/ijms16035635
Luu, T.T., J.N. Søndergaard, L. Peña-Pérez, S. Kharazi, A. Krstic, S. Meinke, L. Schmied, N. Frengen, Y. Heshmati, M. Kierczak, et al. 2022. FOXO1 and FOXO3 cooperatively regulate innate lymphoid cell development. *Front. Immunol.* 13:854312. https://doi.org/10.3389/fimmu.2022.854312
Ma, J., Z. Liu, Y. Wang, Y. Wei, M. Zhao, and S. Wang. 2023. Pulmonary human immune responses in a humanized immune mouse model during influenza virus infection. *The Innovation Life*. 1:100009. https://doi.org/10.59717/j.xinn-life.2023.100009
Marino, F., and M. Cosentino. 2013. Adrenergic modulation of immune cells: An update. *Amino Acids*. 45:55–71. https://doi.org/10.1007/s00726-011-1186-6
Moriyama, S., J.R. Brestoff, A.L. Flamar, J.B. Moeller, C.S.N. Klose, L.C. Rankin, N.A. Yudanin, L.A. Monticelli, G.G. Putzel, H.R. Rodewald, and D. Artis. 2018. β_2-adrenergic receptor-mediated negative regulation of group 2 innate lymphoid cell responses. *Science*. 359:1056–1061. https://doi.org/10.1126/science.aan4829
Muller, P.A., B. Koscsó, G.M. Rajani, K. Stevanovic, M.L. Berres, D. Hashimoto, A. Mortha, M. Leboeuf, X.M. Li, D. Mucida, et al. 2014. Crosstalk between muscularis macrophages and enteric neurons regulates gastrointestinal motility. *Cell*. 158:300–313. https://doi.org/10.1016/j.cell.2014.04.050
Ouyang, W., W. Liao, C.T. Luo, N. Yin, M. Huse, M.V. Kim, M. Peng, P. Chan, Q. Ma, Y. Mo, et al. 2012. Novel Foxo1-dependent transcriptional programs control T(reg) cell function. *Nature*. 491:554–559. https://doi.org/10.1038/nature11581
Schwede, F., E. Maronde, H. Genieser, and B. Jastorff. 2000. Cyclic nucleotide analogs as biochemical tools and prospective drugs. *Pharmacol. Ther.* 87: 199–226. https://doi.org/10.1016/s0163-7258(00)00051-6
Shen, M., Z. Liu, B. Li, Y. Teng, J. Zhang, Y. Tang, S.C. Sun, and H. Liu. 2014. Involvement of FoxO1 in the effects of follicle-stimulating hormone on inhibition of apoptosis in mouse granulosa cells. *Cell Death Dis.* 5:e1475. https://doi.org/10.1038/cddis.2014.400
Sikander, A., S.V. Rana, S.K. Sharma, S.K. Sinha, S.K. Arora, K.K. Prasad, and K. Singh. 2010. Association of alpha 2A adrenergic receptor gene (ADRAlpha2A) polymorphism with irritable bowel syndrome, microscopic and ulcerative colitis. *Clin. Chim. Acta*. 411:59–63. https://doi.org/10.1016/j.cca.2009.10.003
Silveira, W.A., D.A. Gonçalves, J. Machado, N. Lautherbach, D. Lustrino, S. Paula-Gomes, M.G. Pereira, E.H. Miyabara, M. Sandri, I.C. Kettelhut, and L.C. Navegantes. 2020. cAMP-dependent protein kinase inhibits FoxO activity and regulates skeletal muscle plasticity in mice. *FASEB J.* 34:12946–12962. https://doi.org/10.1096/fj.201902102RR
Smillie, C.S., M. Biton, J. Ordovas-Montanes, K.M. Sullivan, G. Burgin, D.B. Graham, R.H. Herbst, N. Rogel, M. Slyper, J. Waldman, et al. 2019. Intra- and inter-cellular rewiring of the human colon during ulcerative colitis. *Cell*. 178:714–730.e22. https://doi.org/10.1016/j.cell.2019.06.029
Spits, H., D. Artis, M. Colonna, A. Diefenbach, J.P. Di Santo, G. Eberl, S. Koyasu, R.M. Locksley, A.N. McKenzie, R.E. Mebius, et al. 2013. Innate lymphoid cells--a proposal for uniform nomenclature. *Nat. Rev. Immunol.* 13:145–149. https://doi.org/10.1038/nri3365
Squair, J.W., M. Gautier, C. Kathe, M.A. Anderson, N.D. James, T.H. Hutson, R. Hudelle, T. Qaiser, K.J.E. Matson, Q. Barraud, et al. 2021. Confronting false discoveries in single-cell differential expression. *Nat. Commun.* 12: 5692. https://doi.org/10.1038/s41467-021-25960-2
Stone, E.L., M. Pepper, C.D. Katayama, Y.M. Kerdiles, C.Y. Lai, E. Emslie, Y.C. Lin, E. Yang, A.W. Goldrath, M.O. Li, et al. 2015. ICOS coreceptor signaling inactivates the transcription factor FOXO1 to promote Tfh cell differentiation. *Immunity*. 42:239–251. https://doi.org/10.1016/j.immuni.2015.01.017
Sun, Y., L. Li, R. Xie, B. Wang, K. Jiang, and H. Cao. 2019. Stress triggers flare of inflammatory bowel disease in children and adults. *Front Pediatr.* 7: 432. https://doi.org/10.3389/fped.2019.00432

Talbot, J., P. Hahn, L. Kroehling, H. Nguyen, D. Li, and D.R. Littman. 2020. Feeding-dependent VIP neuron-ILC3 circuit regulates the intestinal barrier. *Nature*. 579:575–580. https://doi.org/10.1038/s41586-020-2039-9

Thaker, P.H., L.Y. Han, A.A. Kamat, J.M. Arevalo, R. Takahashi, C. Lu, N.B. Jennings, G. Armaiz-Pena, J.A. Bankson, M. Ravoori, et al. 2006. Chronic stress promotes tumor growth and angiogenesis in a mouse model of ovarian carcinoma. *Nat. Med.* 12:939–944. https://doi.org/10.1038/nm1447

Udit, S., K. Blake, and I.M. Chiu. 2022. Somatosensory and autonomic neuronal regulation of the immune response. *Nat. Rev. Neurosci.* 23:157–171. https://doi.org/10.1038/s41583-021-00555-4

Veiga-Fernandes, H., and D. Mucida. 2016. Neuro-immune interactions at barrier surfaces. *Cell*. 165:801–811. https://doi.org/10.1016/j.cell.2016.04.041

Vivier, E., D. Artis, M. Colonna, A. Diefenbach, J.P. Di Santo, G. Eberl, S. Koyasu, R.M. Locksley, A.N.J. McKenzie, R.E. Mebius, et al. 2018. Innate lymphoid cells: 10 Years on. *Cell*. 174:1054–1066. https://doi.org/10.1016/j.cell.2018.07.017

Wallrapp, A., P.R. Burkett, S.J. Riesenfeld, S.J. Kim, E. Christian, R.E. Abdulnour, P.I. Thakore, A. Schnell, C. Lambden, R.H. Herbst, et al. 2019. Calcitonin gene-related peptide negatively regulates alarmin-driven type 2 innate lymphoid cell responses. *Immunity*. 51:709–723.e6. https://doi.org/10.1016/j.immuni.2019.09.005

Wallrapp, A., S.J. Riesenfeld, P.R. Burkett, R.E. Abdulnour, J. Nyman, D. Dionne, M. Hofree, M.S. Cuoco, C. Rodman, D. Farouq, et al. 2017. The neuropeptide NMU amplifies ILC2-driven allergic lung inflammation. *Nature*. 549:351–356. https://doi.org/10.1038/nature24029

Wang, S., P. Xia, Y. Chen, Y. Qu, Z. Xiong, B. Ye, Y. Du, Y. Tian, Z. Yin, Z. Xu, and Z. Fan. 2017. Regulatory innate lymphoid cells control innate intestinal inflammation. *Cell*. 171:201–216.e18. https://doi.org/10.1016/j.cell.2017.07.027

Wang, S., P. Xia, G. Huang, P. Zhu, J. Liu, B. Ye, Y. Du, and Z. Fan. 2016. FoxO1-mediated autophagy is required for NK cell development and innate immunity. *Nat. Commun.* 7:11023. https://doi.org/10.1038/ncomms11023

Zaiss, D.M.W., and P.J. Coffer. 2018. Forkhead box transcription factors as context-dependent regulators of lymphocyte homeostasis. *Nat. Rev. Immunol.* 18:703–715. https://doi.org/10.1038/s41577-018-0048-9

Zheng, P.Y., B.S. Feng, C. Oluwole, S. Struiksma, X. Chen, P. Li, S.G. Tang, and P.C. Yang. 2009. Psychological stress induces eosinophils to produce corticotrophin releasing hormone in the intestine. *Gut*. 58:1473–1479. https://doi.org/10.1136/gut.2009.181701

Zhou, L., W. Zhou, A.M. Joseph, C. Chu, G.G. Putzel, B. Fang, F. Teng, M. Lyu, H. Yano, K.I. Andreasson, et al. 2022. Group 3 innate lymphoid cells produce the growth factor HB-EGF to protect the intestine from TNF-mediated inflammation. *Nat. Immunol.* 23:251–261. https://doi.org/10.1038/s41590-021-01110-0

Zhou, W., and G.F. Sonnenberg. 2020. Activation and suppression of group 3 innate lymphoid cells in the gut. *Trends Immunol.* 41:721–733. https://doi.org/10.1016/j.it.2020.06.009

Supplemental material

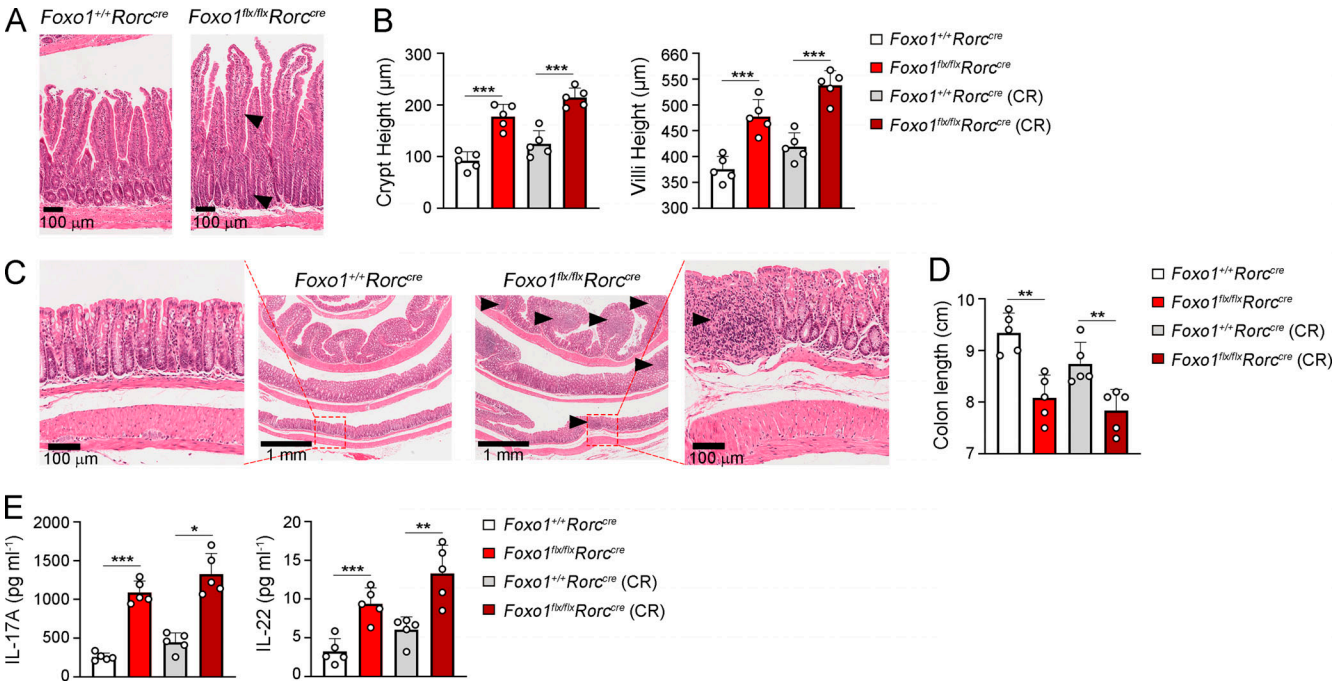

Figure S1. **FOXO1 deficiency in ILC3s and Th17 cells results in intestinal inflammation. (A)** Representative H&E staining of the small intestine sections from *Foxo1*$^{+/+}$*;Rorc-Cre* mice and *Foxo1*$^{flx/flx}$*;Rorc-Cre* mice. Arrowheads indicated the inflammatory lesions. Scale bars, 100 μm. **(B)** Comparison of the small intestine crypt height and villus height between *Foxo1*$^{+/+}$*;Rorc-Cre* mice and *Foxo1*$^{flx/flx}$*;Rorc-Cre* mice with or without CR infection. The indicated mice were gavaged orally by 2 × 10^9 CFU of CR in 200 μl PBS. After 8 d, the heights of crypts and villi were measured and shown as means ± SD. ***, P < 0.001, by two-tailed unpaired Student's *t* test. *n* = 5 for each group. **(C)** Representative H&E staining of the colon sections from *Foxo1*$^{+/+}$*;Rorc-Cre* mice and *Foxo1*$^{flx/flx}$*;Rorc-Cre* mice. Arrowheads indicate the inflammatory lesions. Scale bars are shown as indicated. **(D)** Comparison of the colon length between *Foxo1*$^{+/+}$*;Rorc-Cre* mice and *Foxo1*$^{flx/flx}$*;Rorc-Cre* mice with or without CR infection. The colon length was measured and shown as means ± SD. **, P < 0.01, by two-tailed unpaired Student's *t* test. *n* = 5 for each group. **(E)** Serum levels of IL-17A and IL-22 from *Foxo1*$^{+/+}$*;Rorc-Cre* mice and *Foxo1*$^{flx/flx}$*;Rorc-Cre* mice with or without CR infection were measured by ELISA and shown as means ± SD. *, P < 0.05, **, P < 0.01, ***, P < 0.001, by two-tailed unpaired Student's *t* test. *n* = 5 for each group. Data represent at least three independent experiments.

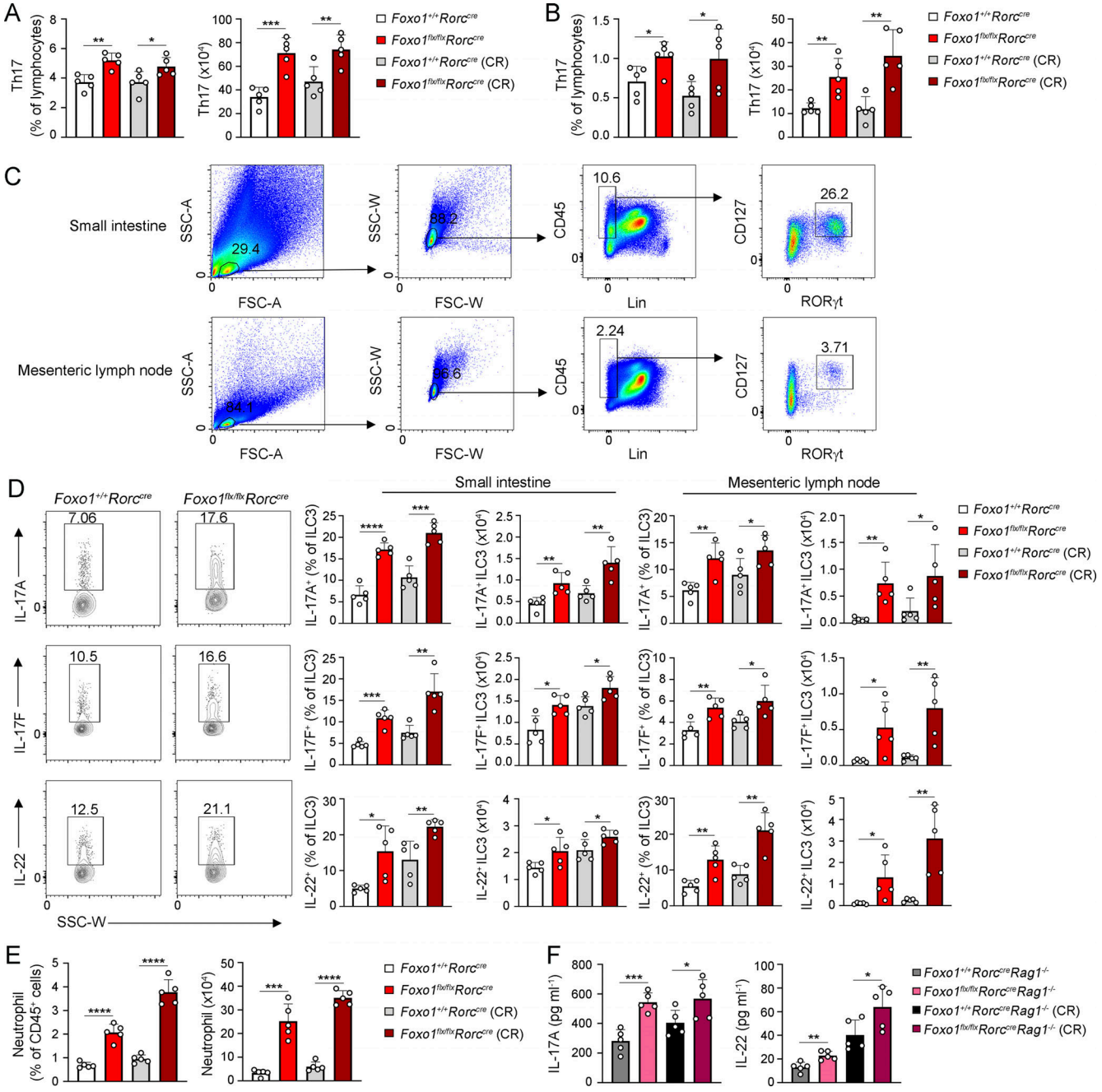

Figure S2. **FOXO1 suppresses the expression of inflammatory cytokines in ILC3s. (A and B)** FOXO1 deficiency promoted the proliferation of Th17 cells. The proportion and numbers of Th17 cells in the small intestine (A) and mesenteric lymph nodes (B) from *Foxo1*$^{+/+}$*;Rorc-Cre* mice and *Foxo1*$^{flx/flx}$*;Rorc-Cre* mice with or without oral gavage of 2 × 10^9 CFU of CR for 8 d. The cell frequency and cell numbers of Th17 cells were analyzed by flow cytometry and shown as means ± SD. *, P < 0.05, **, P < 0.01, ***, P < 0.001, by two-tailed unpaired Student's *t* test. *n* = 5 for each group. **(C)** Gating strategies for mouse ILC3 analysis in small intestine and mesenteric lymph nodes by flow cytometry. **(D)** The proportion and numbers of IL-17A–, IL-17F–, and IL-22–positive ILC3s in small intestine and mesenteric lymph nodes from *Foxo1*$^{+/+}$*;Rorc-Cre* mice and *Foxo1*$^{flx/flx}$*;Rorc-Cre* mice with or without CR infection were analyzed by flow cytometry and shown as means ± SD. The representative flow cytometry plots of ILC3s from uninfected mice are shown on the left. *, P < 0.05, **, P < 0.01, ***, P < 0.001, ****, P < 0.0001, by two-tailed unpaired Student's *t* test. *n* = 5 for each group. **(E)** The proportion and numbers of neutrophils in the small intestine of *Foxo1*$^{+/+}$*;Rorc-Cre* mice and *Foxo1*$^{flx/flx}$*;Rorc-Cre* mice with or without CR infection were analyzed by flow cytometry and shown as means ± SD. ***, P < 0.001, ****, P < 0.0001, by two-tailed unpaired Student's *t* test. *n* = 5 for each group. **(F)** Serum levels of IL-17A and IL-22 from *Foxo1*$^{+/+}$*;Rorc-Cre;Rag1*$^{-/-}$ mice and *Foxo1*$^{flx/flx}$*;Rorc-Cre;Rag1*$^{-/-}$ mice with or without oral gavage of 2 × 10^9 CFU of CR were measured by ELISA and shown as means ± SD. *, P < 0.05, **, P < 0.01, ***, P < 0.001, by two-tailed unpaired Student's *t* test. *n* = 5 for each group. Gate strategies are: Th17 cells = CD3$^+$CD45$^+$CD4$^+$RORγt$^+$. ILC3 = Lin$^-$NK1.1$^-$KLRG1$^-$CD45$^+$CD127$^+$RORγt$^+$. Neutrophil = CD3$^-$CD19$^-$CD45$^+$CD11b$^+$Gr-1$^+$. Data represent at least three independent experiments.

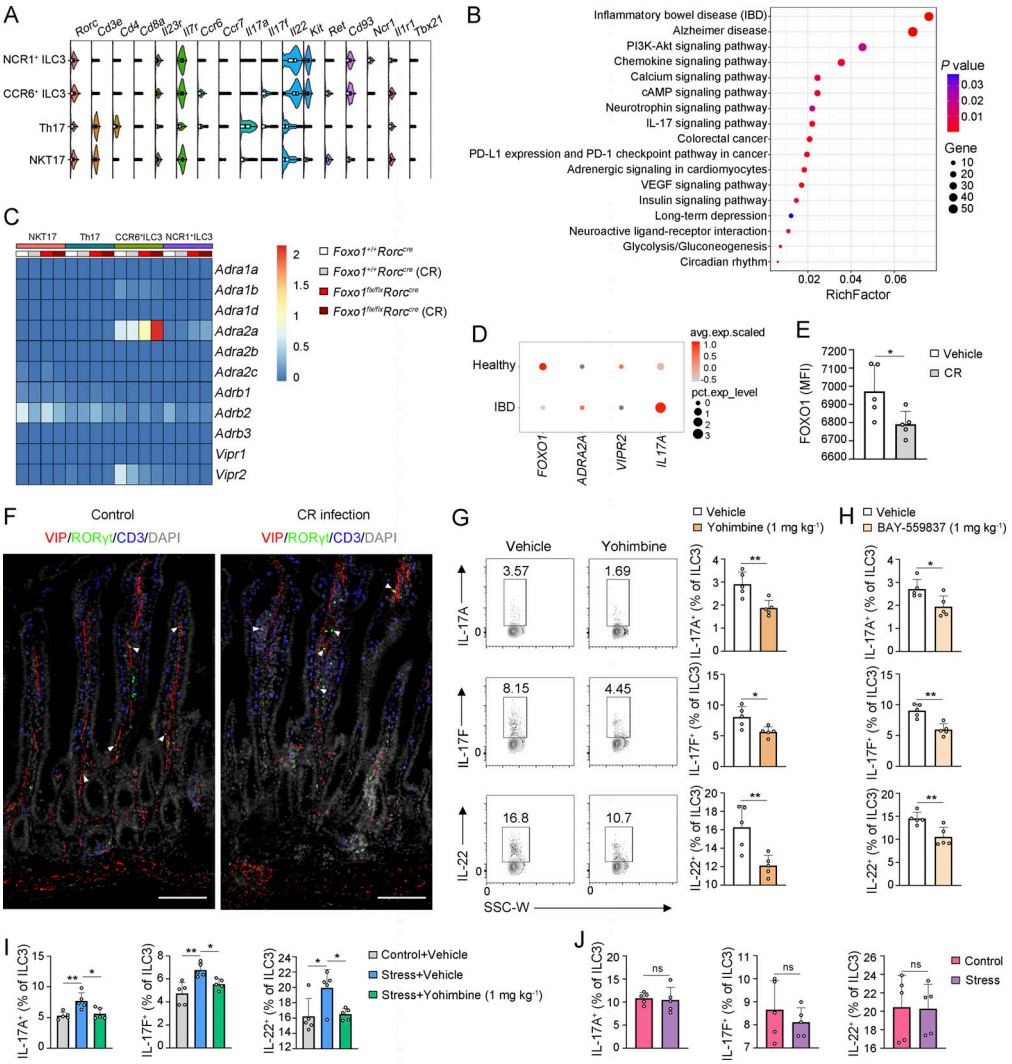

Figure S3. **FOXO1 regulates ADRA2A and VIPR2 signaling in ILC3s. (A)** scRNA-seq revealed the subpopulation of ILC3s and Th17 cells. CD3$^+$ cells (Lin$^-$CD45$^+$CD3$^+$, Lin = CD19, CD11b, CD11c, TER-119, Gr-1) and ILC3s (Lin$^-$CD3$^-$CD45^{low}CD127$^+$CD90^{hi}) from lamina propria of the small intestine of *Foxo1*$^{+/+}$*;Rorc-Cre* mice and *Foxo1*$^{flx/flx}$*;Rorc-Cre* mice with or without CR infection were isolated and examined using scRNA-seq. *Rorc*-positive cells were selected out and clustered partitioned into four clusters, including Th17 (marked by high expression of *Rorc*, *Cd3e*, *Cd4*, *Il7r*, *Ccr6*, *Il17a*, *Il22*, *Il1r1*, et al.), CCR6$^+$ ILC3 (marked by scant expression of *Cd3e*, and high expression of *Rorc*, *Kit*, *Il23r*, *Il7r*, *Ccr6*, *Ret*, *Cd93*, *Il17f*, *Il22*, *Il1r1*, et al.), NCR1$^+$ ILC3 (marked by scant expression of *Cd3e*, and high expression of *Rorc*, *Kit*, *Il23r*, *Il7r*, *Ncr1*, *Cd93*, *Il22*, *Il1r1*, et al.), and NKT17 (marked by scant expression of *Cd4*, *Cd8a*, and high expression of *Rorc*, *Cd3e*, *Kit*, *Il23r*, *Il7r*, *Ret*, *Cd93*, *Il17a*, *Il22*, *Il1r1*, et al.). Violin plots displaying the expression of signature genes in each cell cluster. **(B)** Enrichment analysis of Kyoto Encyclopedia of Genes and Genomes pathways of DEGs only in ILC3s, not in Th17 cells of *Foxo1*$^{flx/flx}$*;Rorc-Cre* mice versus *Foxo1*$^{+/+}$*;Rorc-Cre* mice after CR infection. RichFactor = (the number of DEGs)/(total number of genes). **(C)** Heatmap showed the normalized expression of the indicated genes in Th17, CCR6$^+$ ILC3, NCR1$^+$ ILC3, and NKT17 cells from *Foxo1*$^{+/+}$*;Rorc-Cre* mice and *Foxo1*$^{flx/flx}$*;Rorc-Cre* mice with or without CR infection. **(D)** Dot plot showed the mean expression levels of the indicated genes in ILC3s from healthy donors and IBD patients from scRNA-seq data of previous studies (Smillie et al., 2019). The dot size represented the level of the proportion of cells that expressed the indicated genes. The color represented the average expression level of indicated genes across ILC3s. **(E)** Expression level of FOXO1 in ILC3s from mice with or without CR infection was analyzed by flow cytometry. MFI of FOXO1 are shown as means ± SD. *, P < 0.05, by two-tailed unpaired Student's *t* test. *n* = 5 for each group. **(F)** Immunofluorescence staining of the localization of VIP (red) and ILC3s (green) in the small intestine from RORγt-GFP mice with (right) or without (left) CR infection. Scale bars, 100 µm. **(G)** WT mice were i.p. injected with vehicle or ADRA2A antagonist Yohimbine (1 mg kg^{-1} mouse) and sacrificed after 24 h. The proportion of IL-17A–, IL-17F–, and IL-22–positive ILC3s from the small intestine were determined by flow cytometry and shown as means ± SD. The representative flow cytometry plots of intestinal ILC3s are shown on the left panel. *, P < 0.05, **, P < 0.01, by two-tailed unpaired Student's *t* test. *n* = 5 for each group. **(H)** WT mice were treated with vehicle or VIPR2 agonist BAY-559837 (1 mg kg^{-1} mouse) via i.p. injection and sacrificed after 24 h. The proportion of IL-17A–, IL-17F–, and IL-22–positive ILC3s from the small intestine were determined by flow cytometry and shown as means ± SD. *, P < 0.05, **, P < 0.01, by two-tailed unpaired Student's *t* test. *n* = 5 for each group. **(I)** WT mice were placed in 50-ml conical centrifuge tubes with ventilation holes for 4 h per day for 29 d followed by vehicle or ADRA2A antagonist Yohimbine (1 mg kg^{-1} mouse) treatment and sacrificed after 24 h. The proportion of IL-17A–, IL-17F–, and IL-22–positive ILC3s from the small intestine were determined by flow cytometry and shown as means ± SD. *, P < 0.05, **, P < 0.01, by one-way ANOVA. *n* = 5 for each group. **(J)** *Foxo1*$^{flx/flx}$*;Rorc-Cre;Rag1*$^{-/-}$ mice were placed in 50-ml conical centrifuge tubes with ventilation holes for 4 h per day for 29 d to generate chronic stress model. The proportion of IL-17A–, IL-17F–, and IL-22–positive ILC3s in the small intestine from control and stressed mice were determined by flow cytometry and shown as means ± SD. ns, not significant, by two-tailed unpaired Student's *t* test. *n* = 5 for each group. ILC3 = Lin$^-$NK1.1$^-$KLRG1$^-$CD45$^+$CD127$^+$RORγt$^+$. **(A–C)** Data represent at least two independent experiments. **(E–I)** Data represent at least three independent experiments.

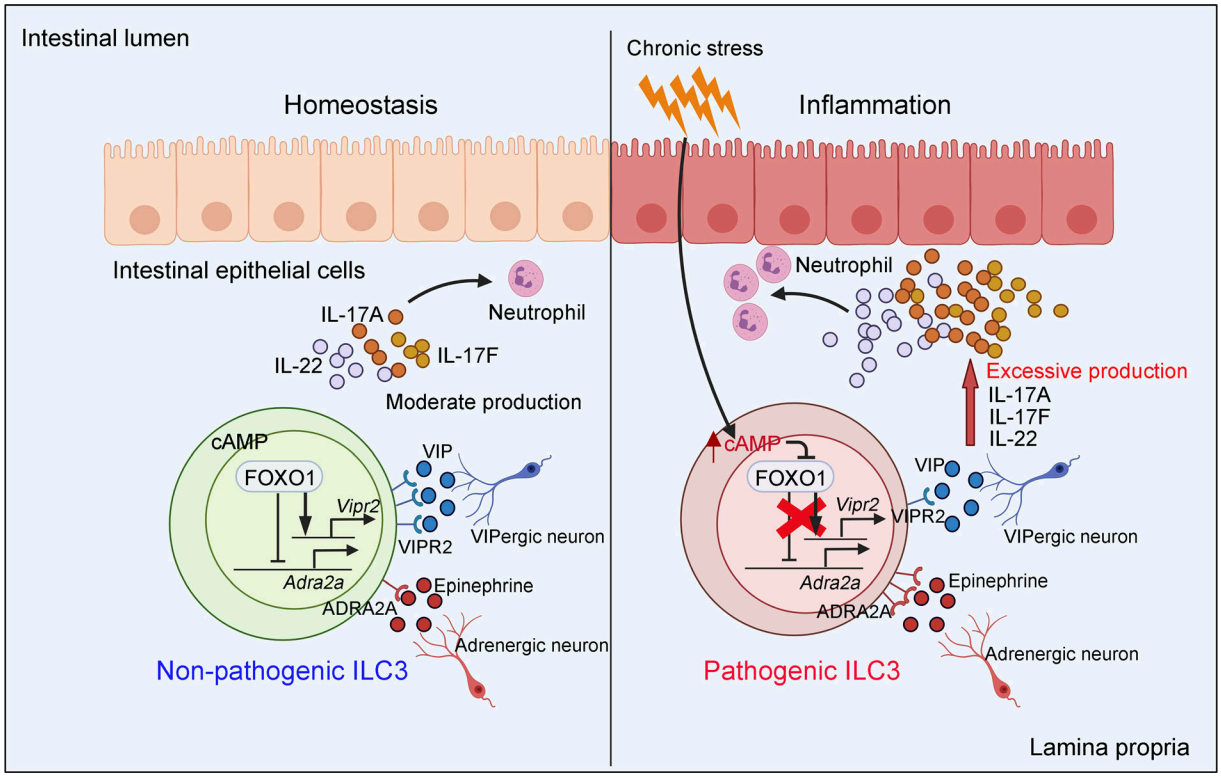

Figure S4. **Work model for FOXO1-induced neuronal signaling regulation of ILC3s in the intestine.** FOXO1 suppressed hyperactivation of ILC3s by balancing VIP and adrenergic signaling to maintain intestinal homeostasis. CCR6$^+$ ILC3s express high levels of *Adra2a* and *Vipr2*, indicating that FOXO1 might mainly regulate CCR6$^+$ ILC3s.

Provided online are two tables. Table S1 shows the quality control metrics of scRNA-seq data. Table S2 shows the colitis-related gene set.